



HAL
open science

On the elusive nature of Carbopol gels: “model”, weakly thixotropic, or time-dependent viscoplastic materials?

Eliane Younes, Michal Himl, Zdenek Stary, Volfango Bertola, Teodor Burghilea

► To cite this version:

Eliane Younes, Michal Himl, Zdenek Stary, Volfango Bertola, Teodor Burghilea. On the elusive nature of Carbopol gels: “model”, weakly thixotropic, or time-dependent viscoplastic materials?. *Journal of Non-Newtonian Fluid Mechanics*, 2020, 281, pp.104315. 10.1016/j.jnnfm.2020.104315 . hal-02865265

HAL Id: hal-02865265

<https://hal.science/hal-02865265>

Submitted on 25 Nov 2020

HAL is a multi-disciplinary open access archive for the deposit and dissemination of scientific research documents, whether they are published or not. The documents may come from teaching and research institutions in France or abroad, or from public or private research centers.

L'archive ouverte pluridisciplinaire **HAL**, est destinée au dépôt et à la diffusion de documents scientifiques de niveau recherche, publiés ou non, émanant des établissements d'enseignement et de recherche français ou étrangers, des laboratoires publics ou privés.

On the elusive nature of Carbopol gels: “*model*”, weakly thixotropic, or time-dependent viscoplastic materials?

Eliane Younes

Université de Nantes, CNRS, Laboratoire de Thermique et Energie de Nantes, UMR 6607, La Chantrerie, Rue Christian Pauc, B.P. 50609, F-44306 Nantes Cedex 3, France

Michal Himl

Department of Organic Chemistry, University of Chemical Technology Prague, Technická 1905/5, 166 28 Prague, Czech Republic

Zdenek Stary

Institute of Macromolecular Chemistry Czech Academy of Sciences, Heyrovského nam. 2, 162 06 Prague, Czech Republic

Volfango Bertola

Laboratory of Technical Physics, School of Engineering, University of Liverpool, Liverpool, L69 3GH, United Kingdom

Teodor Burghelea

Université de Nantes, CNRS, Laboratoire de Thermique et Energie de Nantes, UMR 6607, La Chantrerie, Rue Christian Pauc, B.P. 50609, F-44306 Nantes Cedex 3, France

Abstract

The question of whether Carbopol gels always behave as “*model*” yield stress material is addressed experimentally. Prompted by several simple hydrodynamic experiments performed with Carbopol gels that can not be fully understood within the commonly accepted “*model*” picture, we revisit the yielding behaviour of a Carbopol gel. When subjected to a loading/unloading process, the yielding of the Carbopol is gradual and exhibits a rheological

Email addresses: Eliane.Younes@univ-nantes.fr (Eliane Younes), michal.himl@vscht.cz (Michal Himl), stary@imc.cas.cz (Zdenek Stary), Volfango.Bertola@liverpool.ac.uk (Volfango Bertola), Teodor.Burghelea@univ-nantes.fr (Teodor Burghelea)

hysteresis. By in-situ visualisation of the microstructure it is demonstrated that these features do not originate from a micro-structural damage of the micro-gel. A systematic description of the role of the rate at which the material is forced (loaded or unloaded) on the yielding scenario is given. In closing, the question of how simple a scalar model can be and yet accurately describe the experimentally observed yielding scenario of a Carbopol gel in a rheometric flow is addressed. It is concluded that simple scalar models may do such job as long as they are not too simple and include a minimal amount of physical ingredients.

Contents

1	Introduction	7
1.1	Carbopol gels as “ <i>model</i> ” yield stress materials	8
1.2	Three simple hydrodynamic experiments at odds with the “ <i>model</i> ” yield stress picture of a Carbopol gel	8
1.2.1	Sedimentation of a spherical solid object in a Carbopol gel	10
1.2.2	The Landau-Levich flow	12
1.2.3	Rayleigh-Bénard thermo-convective instability	13
2	Experimental methods	14
2.1	Fluid preparation	14
2.2	Rheological measurements	14
2.3	Micro-rheo digital particle image velocimetry observations of the rheometric flow	16
3	Results	17
3.1	Yielding of a Carbopol gel to stress revisited	17
3.2	Visualisation of the Carbopol microstructure	19
3.3	On the physical reasons behind the emergence of the rheological hysteresis during the loading/unloading of the Carbopol sample	22
3.4	Role of the rate of the forcing on the dynamics of the solid-fluid transition	23
3.5	On modelling the yielding transition in a Carbopol gel: how simple a rheological model can get (and yet remain meaningful)?	26
3.5.1	Applicability of the model proposed in Ref. [9] in describing the rheological response of a Carbopol gel . . .	28
3.5.2	Applicability of the model proposed in Ref. [33] in describing the rheological response of a Carbopol gel .	32
4	Conclusions, outlook	37
5	Author contributions	38
6	Acknowledgements	38

List of Figures

1	Dependence of the rate of deformation on the imposed stress measured during a linear stress ramp. The empty/full symbols refer to the increasing/decreasing branch of the ramp. The vertical dashed line separates the solid deformation regime (S) and the fluid deformation regime (F). The full line is a nonlinear fit by the Herschel-Bulkley model.	9
2	(a) Experimentally measured flow pattern around a solid sphere of radius $R = 1.95 \text{ mm}$ freely falling through a 0.07% (wt) solution of Carbopol 980. The Reynolds number is $Re = 0.087$. The plot is adapted from Fig. 8 of Ref. [34]. panel (b) Numerical flow pattern obtained by Fraggedakis and coworkers - adapted with permission from Ref. [22] (courtesy of Professor John Tsamopoulos).	11
3	In-situ visualisation of the flow field around a rigid plate withdrawn at a constant speed U_p from a container filled with a 0.2% (wt) solution of Carbopol 980. The Reynolds number was $Re = 0.05$	12
4	Instantaneous flow field measured right above the onset of the Rayleigh-Bénard convection in a Carbopol gel heated from below. The plot is adapted from Ref. [26].	13
5	Schematic representation of the linear stepped stress ramp. For clarity of the presentation, we have chosen here $N = 20$ steps of each of the two branches of the ramp while during the experiments we report herein $N = 500$	15
6	(a) Schematic representation (not in scale) of the micro-rheo-PIV system used to measure the dependence of the tangential velocity component at $r = 5R/6$ (R being the radius of the plate used during the rheological tests) on the vertical coordinate z . (b) Photograph of the serrated transparent disk used for the micro-rheo-PIV measurements.	16

7	Dependence of the absolute value of the rate of shear $ \dot{\gamma} $ on the reduced applied stress τ/τ_y measured for increasing (empty symbols) and decreasing (full symbols) imposed stresses. The stresses were varied linearly in time and the characteristic forcing time was $t_0 = 1.5$ s. The vertical dashed lines separate the three deformation regimes: (S) - solid, (S+F) - intermediate and (F) - fluid. The full square marks the point of elastic recoil (the rate of shear changes sign) systematically observed on the decreasing stress branch of the ramp. The full line is a fit by the Herschel-Bulkley model.	18
8	Fluorescent micro-graph of a 0.1% (wt) solution of Carbopol 980 containing a $10^{-5}M$ aqueous solution of molecular Rhodamine 6G at (a) $pH = 3$ (no measurable yield stress). (b) $pH = 7$ (measurable yield stress).	20
9	(a) Molecular structure of Rhodamine 6G used by Dinkgreve and coworkers in Ref. [16]. (b) Molecular structure of Rhodamine <i>B</i> used in the present study.	21
10	Micrograph of the neutral Carbopol gel covalently labelled with Rhodamine <i>B</i> (see text for description). The bright details of the micrograph refer to the Carbopol particles while the dark details refer to the aqueous solvent.	21
11	(a) Time averaged (over 500 instantaneous velocity fields) velocity field. The false colour map refers to the magnitude of the velocity. (b) Dependence of the time averaged azimuthal velocity component U on the vertical coordinate z . The error bars are defined by the root mean square deviation obtained by performing a statistical analysis over 500 instantaneous flow fields and do not exceed 7% of the measured value.	23
12	12(a) Dependence of the rate of strain $\dot{\gamma}$ on the imposed stress measured on the increasing branch of the stress ramp for various values of the characteristic forcing time t_0 . 12(b) Dependence of the absolute value of the rate of strain $ \dot{\gamma} $ on the imposed stress measured on the decreasing branch of the stress ramp for various values of the characteristic forcing time t_0 . In both panels, the top colour bar maps the value of t_0 . The vertical dashed lines separate the solid deformation regime (S) the intermediate regime (S+F) and the fluid deformation regime (F) . The full line is a nonlinear fit by the Herschel-Bulkley model.	24

13	Dependence of the shear rate plateau value $ \dot{\gamma}_0 $ on the characteristic forcing time t_0 measured on the increasing ramp (circles) and the decreasing branch of the stress ramp (squares). The full line is a power law fit, $\dot{\gamma}_0 = 10^{-4} + 7 \cdot 10^{-4} t_0^{-1.06}$. The dashed line is a power law fit, $\dot{\gamma}_0 = 10^{-4} + 0.0018 t_0^{-1.05}$	25
14	Dependence of the magnitude of the rheological hysteresis on the characteristic forcing time t_0 . The full line is a guide for the eye, $A \propto 1/t_0$	26
15	Response of the model proposed in Ref. [9] to a ramp in the shear rate (see text for details): (a) Dependence of the micro-structural parameter Φ on the imposed shear rate $\dot{\gamma}$. (b) Dependence of the reduced stress τ/τ_y on the imposed shear rate $\dot{\gamma}$. The dashed line is a guide for the eye, $\tau/\tau_y \propto \dot{\gamma}$ which is the Newtonian asymptotic limit of the model. (c) Dependence of the viscosity η on the imposed shear rate $\dot{\gamma}$. The dashed line is a guide for the eye, $\eta \propto \dot{\gamma}^{-1}$. (d) Dependence of the viscosity η on the reduced stress τ/τ_y . The various colours in each panel refer to the initial condition of the micro-structural parameter $\Phi(0)$ mapped onto the top colour-bar. The full lines and the full symbols in each panel refer to the increasing branch of the ramp while the dashed-dotted lines refer to the decreasing branch of the ramp.	31
16	(a) Dependence of the structural parameter Φ on the applied stress obtained by solving numerically the elasto-viscoplastic model proposed by Putz and Burghelca, [33] for an increasing/decreasing stress ramp with $\tau_{max} = 20Pa$ and $t_0 = 1.5 s$. (b) Best fit of the dependence of the shear rate $ \dot{\gamma} $ on the reduced applied stress τ/τ_y . In both panels the full/dash-dotted lines refer to the the increasing/decreasing branch of the linear stress ramp.	35
17	Stress overshoot observed during a step in the rate of shear $\dot{\gamma}(t) = H(t)\dot{\gamma}_{max}$: (a) Time dependence of the reduced stress τ/τ_y . The full lines are the numerical solutions of the model proposed in Ref. [33]. (b) Time dependence of structural parameter Φ . In both panels the symbols are: circles - $\dot{\gamma}_{max} = 0.5s^{-1}$, squares - $\dot{\gamma}_{max} = 1.5s^{-1}$, right triangles - $\dot{\gamma}_{max} = 2s^{-1}$, left triangles - $\dot{\gamma}_{max} = 3s^{-1}$	36

1. Introduction

For many years since the synthesis of carbomer polymers in the 1950's [Brown, H.P., Carboxylic polymers, US Patent 2798053A, 1957], aqueous Carbopol dispersions have been considered a reference standard for a "*model*" yield stress fluid, specifically a fluid that perfectly matches the behaviour predicted by yield-stress fluid constitutive models, such as the Herschel-Bulkley model. This is quite a remarkable exception, since normally constitutive equations attempt at mimicking the flow behaviour within a limited range of flow parameters, and not vice-versa. As the rheometers technology became more and more sophisticated, however, concerns about the fidelity of Carbopol gels in modeling the yield-stress fluids behaviour have been equally growing in number and strength. Echos of the fiery debate about the existence of the yield-stress in the 1990's [5, 4] are still haunting the viscoplastic fluids community. More recently, an equally intense controversy has flourished about the concept itself of "*model*" yield-stress fluids. On one hand, some authors show that Carbopol gels are indeed the simple model yield-stress fluid that many people believe them to be, [11, 31, 30]. On the other hand, however, other authors report experimental evidence of behaviours that significantly depart from that of a model yield-stress fluid, such as rheological hysteresis in the flow curve [17, 19, 33, 43], transient shear banding [20] that persists for a very long time, stress overshoot during steps in the rate of strain [18] and the breaking of fore-aft symmetry in a falling ball experiment, [34].

Most recently, it was suggested that both types of behaviour may be found in the same type of Carbopol, depending on the preparation protocol [16]: strong stirring breaks the polymers into smaller fragments, some of which are so small that they exhibit Brownian motion. This generates a depletion interaction that leads to gel formation, which in turn leads to the thixotropy, and is usually interpreted in terms of a simple toy-model for the evolution of the microstructure and the viscosity, [27]. The basic assumptions of the model are that there exists a scalar structural parameter, Φ , that describes the local degree of interconnection of the microstructure, and that the viscosity increases with increasing Φ . In addition, for an ageing system at low or zero shear rate Φ increases, while the flow at sufficiently high shear rates breaks down the structure and Φ decreases to a low steady state value.

The present work aims to offer a contribution to the settlement of this dispute regarding the elusive nature of Carbopol gels by combining macro-rheological experiments, in-situ visualisation of the Carbopol micro-structure and phenomenological modeling.

The paper is organised as follows. Following a general introduction, we

describe the “*model*” yield stress material picture of a Carbopol gel, Sec. 1.1. Next, we highlight three distinct simple hydrodynamic experiments that are at odds with this ideal picture, Sec. 1.2. The experimental methods including a detailed description of the protocol used to prepare the Carbopol gel are discussed in Sec. 2. The central results of the study are described in Sec. 3. Prompted by these three simple flow examples all at odds with the “*model*” picture, we revisit the yielding picture of a Carbopol gel in Sec. 3.1. The question regarding the micro-structural integrity of the Carbopol sample is addressed in Sec. 3.2. The dependence of the yielding scenario of the Carbopol gel on the rate at which the material is loaded/unloaded is systematically analysed in Sec. 3.4. Finally, we address in Sec. 3.5 the issue of the phenomenological modelling of the yielding process of a Carbopol gel. The paper closes with a summary of the main findings and of the central conclusions of the study, Sec. 4.

1.1. Carbopol gels as “*model*” yield stress materials

We clarify in the following what is commonly understood by the “*model*” yield stress picture commonly attributed to Carbopol gels. To illustrate this picture, a typical dependence of the rate of strain on the applied stress measured with a 0.1% (*wt*) aqueous solution of Carbopol 980 during an increasing/decreasing stress ramp (the full/empty symbols marking each branch of the ramp are hardly distinguishable because they overlap nearly perfectly) performed with a plate-plate geometry is illustrated in Fig. 1.

The rheological data presented in Fig. 1 bear several key features:

1. The transition from a solid regime (**S**) to a fluid regime (**F**) seems to occur at a well defined value of the applied stress equal to the yield stress, $\tau = \tau_y$.
2. The deformation states seem to be fully reproducible upon increasing/decreasing stresses meaning that the material responds exactly the same to an imposed stress during a loading and un-loading process.
3. The yielding process seems to be accurately described by the Herschel-Bulkley constitutive law, $\tau = \tau_y + K|\dot{\gamma}|^n$ - the full line in Fig. 1. Here, K stands for the consistency and $n \in (0, 1)$ for the power law index.

Together with the above enumerated features of the yielding process, Carbopol gels are equally and universally recognised for their chemical and micro-structural stability during extended periods of time.

1.2. Three simple hydrodynamic experiments at odds with the “*model*” yield stress picture of a Carbopol gel

The “*model*” yield stress picture of a Carbopol gel described in Sec. 1.1 may be challenged by (at least) three relatively simple to perform hydrody-

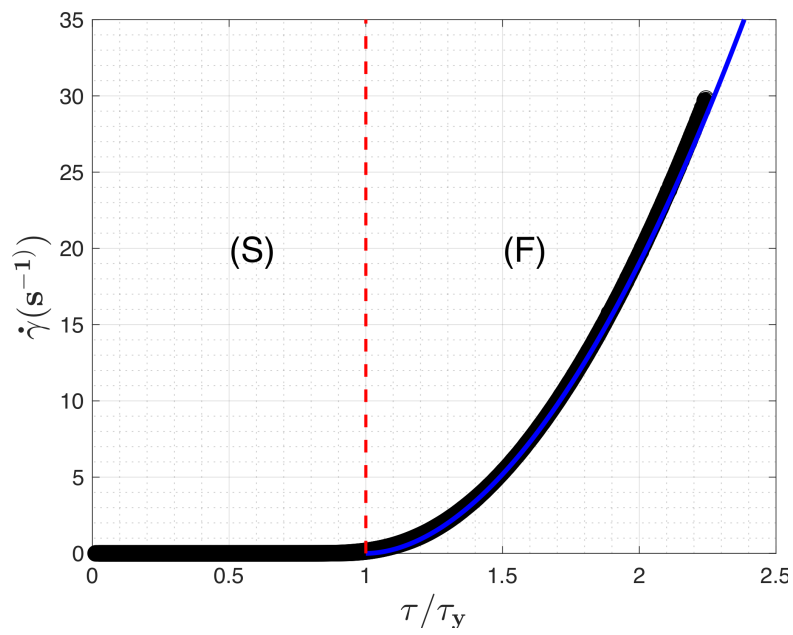


Figure 1: Dependence of the rate of deformation on the imposed stress measured during a linear stress ramp. The empty/full symbols refer to the increasing/decreasing branch of the ramp. The vertical dashed line separates the solid deformation regime (**S**) and the fluid deformation regime (**F**). The full line is a nonlinear fit by the Herschel-Bulkley model.

dynamic experiments which we briefly describe in the following.

1.2.1. Sedimentation of a spherical solid object in a Carbopol gel

The first example refers to the sedimentation of a spherical solid object in a Carbopol gel at low Reynolds numbers ($Re < 1$). In the absence of inertial contributions, the flow pattern around a spherical object moving at constant speed through a “*model*” viscoplastic material should exhibit a fore-aft symmetry, [6]. The measurements of the instantaneous flow fields around the solid object performed by Putz and coworkers [34] revealed a strikingly different picture, Fig. 2(a). First, the fore-aft symmetry was systematically broken for various concentrations of Carbopol and various radii of the falling sphere while validation experiments performed with a purely viscous glycerol solution revealed a purely symmetric flow pattern. Second and perhaps the most intriguing, a negative wake phenomenon was observed: beyond a stagnation point located in the aft region of the flow, the flow direction was reversed, i.e. the fluid was moving away from the falling object. As the Reynolds numbers were small (typically $Re < 1$) such flow patterns do not originate from inertial effects.

A simple phenomenological explanation of the fore-aft symmetry breaking may be given in terms of the thixotropy of the material as follows. The material located in the fore region of the moving solid is subjected to a stress gradually increasing in time. The characteristic time scale associated to this loading process of the material may be estimated as $t_0 = R/U_0$ where R is the radius of the sphere and U_0 its terminal velocity. The material located in the aft region of the flow is subjected to a gradually decreasing stress or, to an unloading process. Thus, the broken symmetry of the flow pattern may be attributed to an irreversibility of the deformation states of the material upon loading/unloading (thixotropy). Two important points have to be made here. First, the measurements of the second invariant of the rate of strain tensor presented in Ref. [34] indicate that the gel is loaded/unloaded around the solid-fluid transition. Second, during all the experiments reported in Ref. [34] the material was loaded/unloaded in an “*unsteady*” fashion: viewed in a Lagrangian frame of reference, the material elements were subjected to a constant stress only for a finite time of the order of $t_0 < 1$ s.

The emergence of the negative wake on the other hand may be explained by the presence of elasticity in the flow and has been systematically described both experimentally and theoretically for the case of viscoelastic fluids, [1, 25]. The “*model*” yield stress picture of a Carbopol gel does not account for any of these two phenomenological behaviours.

A numerical simulation of the sedimentation problem in an elasto-viscoplastic material described by the Saramito model [41] was reported by Fraggidakis

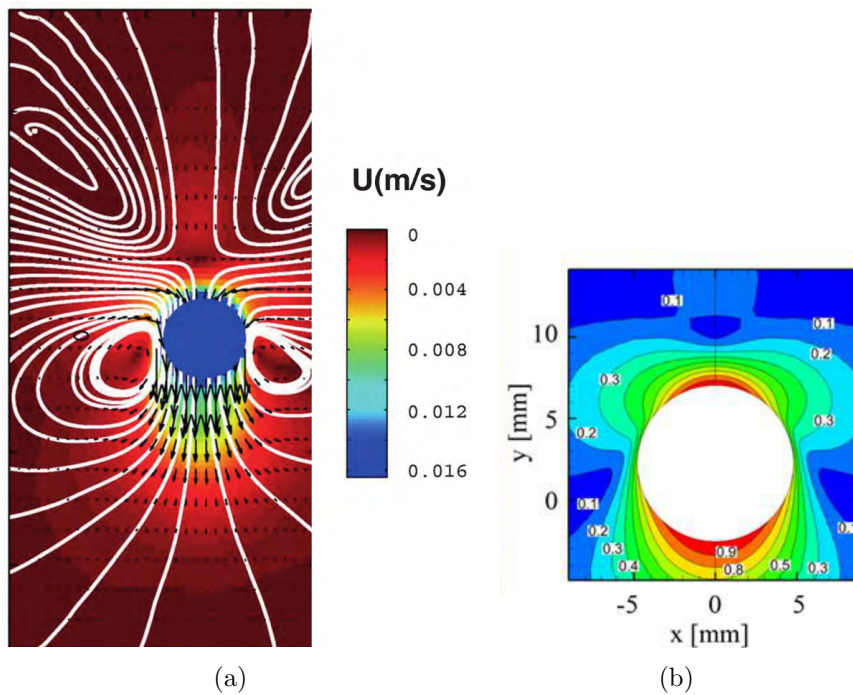


Figure 2: (a) Experimentally measured flow pattern around a solid sphere of radius $R = 1.95 \text{ mm}$ freely falling through a 0.07% (wt) solution of Carbopol 980. The Reynolds number is $Re = 0.087$. The plot is adapted from Fig. 8 of Ref. [34]. panel (b) Numerical flow pattern obtained by Fraggedakis and coworkers - adapted with permission from Ref. [22] (courtesy of Professor John Tsamopoulos).

and coworkers, [22]. The authors report numerical flow patterns qualitatively similar to those obtained experimentally and emphasise the role of elastic effects for both the fore-aft symmetry breaking and the emergence of the negative wake effect.

1.2.2. The Landau-Levich flow

A second simple fluid dynamics experiment somewhat similar to the first one from the point of view of flow kinematics is the Landau-Levich experiment which consists withdrawing a solid plate at a constant speed (sufficiently small so the Reynolds number does not exceed unity, $Re \leq 1$) from a bath filled with a Carbopol gel.

An instantaneous flow pattern measured during a Landau-Levich experiment performed with a 0.2%(wt) solution of Carbopol 980 is shown in Fig. 3. This experiment was performed with a rough plate in order to eliminate the wall slip. The speed of the rigid plate was $U_p = 3\text{mm}/s$.

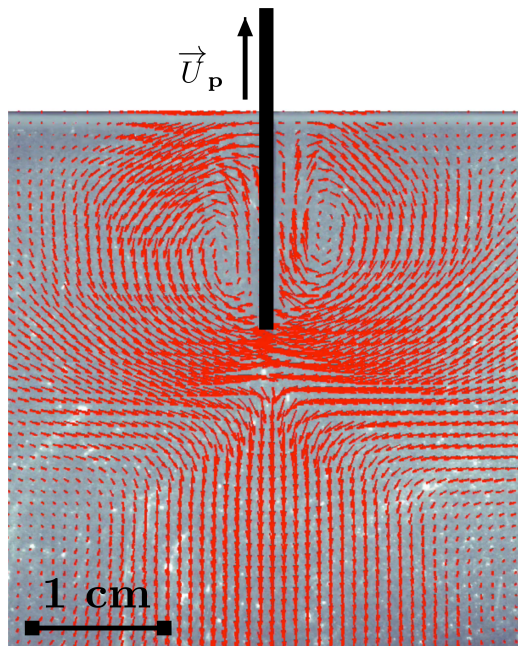


Figure 3: In-situ visualisation of the flow field around a rigid plate withdrawn at a constant speed U_p from a container filled with a 0.2% (wt) solution of Carbopol 980. The Reynolds number was $Re = 0.05$.

As in the case of the sedimentation experiment discussed in Sec. 1.2.1, a negative wake effect is clearly visible. Whereas we are not aware of any numerical simulations that captures this effect, we believe it is once more

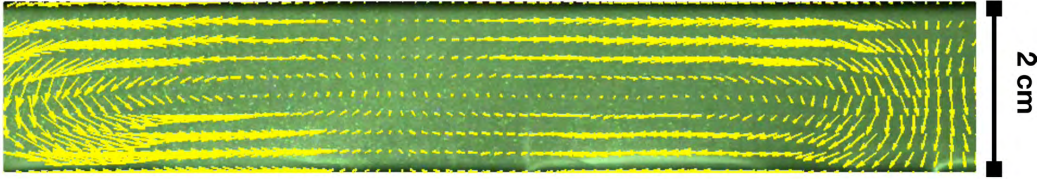


Figure 4: Instantaneous flow field measured right above the onset of the Rayleigh-Bénard convection in a Carbopol gel heated from below. The plot is adapted from Ref. [26].

attributed to the elasticity. We may therefore conclude that this second simple experiment is at odds as well with the “*model*” yield stress picture of a Carbopol gel.

1.2.3. Rayleigh-Bénard thermo-convective instability

A third simple fluid dynamics setting refers to the Rayleigh-Bénard convective instability. For the case of a Newtonian fluid heated from below when the vertical temperature gradient exceeds a critical value such as the buoyancy forces overcome viscous dissipation (or the Rayleigh number Ra exceeds a critical value $Ra_c \approx 1708$) the system loses its hydrodynamic stability and the so called thermal convection is observed.

Zhang and coworkers were the first to investigate the possibility of triggering thermal convection in a yield stress material heated from below, [45].

By means of stability analysis they have demonstrated that, within the framework of the Bingham model, the system is linearly stable. This means that, unlike in the Newtonian case, infinitesimally small perturbations of the flow field and the temperature field are unable to destabilise the flow regardless the value of the Rayleigh number.

A weakly nonlinear stability analysis performed by Balmforth and Rust concludes that, within the framework of the Herschel-Bulkley model and at small Bingham numbers Bn , a sufficiently large finite amplitude perturbation of the base state may destabilise the flow and trigger Rayleigh-Bénard convection, [2].

The experiments performed by Kebiche et al, [26], however, indicate that convective states may be triggered in the absence of a finite amplitude perturbation and the bifurcation towards the convective state is an imperfect bifurcation that may be described by the stationary Landau-Ginzburg model with a field. An instantaneous flow field measured right above the onset of the thermo-convective instability is exemplified in Fig. 4.

The discrepancy between the experimental findings reported in Ref. [26] with the two stability studies reported in Refs. [45, 2] can only be attributed

to the rheological behaviour of the gel around the solid-fluid transition. Indeed, the onset of convection corresponds to very small rates of deformation typically in the range $10^{-4} - 10^{-3}$ (s^{-1}). Within this range of shear rates it is unclear how realistic a simple Herschel-Bulkley type model really is. This issue will be explicitly addressed later on through the paper in Sec. 3.1.

2. Experimental methods

2.1. Fluid preparation

We chose a 0.15%(*wt*) aqueous solution of Carbopol 940. Carbopol is the generic trade name of a cross-linked polyacrylic acid $-[CH_2-CH(COOH)]-$ with high molecular weight. In an anhydrous state, it is commercialised in the form of a white powder soluble in aqueous solvents. After the addition of a neutralising agent such as sodium hydroxide (NaOH), a clear gel is obtained. The Carbopol gels exhibit a yield stress behaviour in a neutral state due to the presence of a jammed spongy microstructure, [28, 24, 33].

The Carbopol gel was prepared according to the following protocol which was very similar to the protocol used by Dinkgreve and coworkers, [16]. First, the right amount of anhydrous Carbopol was dissolved in de-ionized water using a magnetic stirring device at a speed of 1000 *rpm*. The stirring process has been carried on for several hours after an homogeneous solution was obtained. The degree of mixing/dissolution was assessed visually by monitoring the optical isotropy of the solution. Next, the *pH* of the solution was gradually increased from 3.2 to 7 by gradual titration with a small amounts of a 10 *wt%* aqueous *NaOH* solution gradually pipetted while gently mixing the solution. The neutralised mixture has been gently stirred using a propeller mixer for three additional hours. A particular attention was to maintain the speed of the stirrer around 50*rpm* in order to avoid the mechanical damage of the microstructure. After preparation, the batch of the gel was kept in an air-tight container in order to avoid the evaporation of the solvent and allowed to rest at room temperature for 24*h*. A small amount of the solution was covalently labelled with Rhodamine *B* in order to visualise the micro-structure by means of epi-fluorescent microscopy (see Sec. 3.2 for the details). We have tested that the rheological properties of the gel sample were unaltered by the fluorescent labelling.

2.2. Rheological measurements

The rheological measurements were performed using a controlled stress rotational rheometer (Mars *III*, Thermofischer Scientific) equipped with a nano-torque module. Tests were performed using a parallel plate geometry with a diameter $D = 35$ *mm* and a gap $d = 1$ *mm*. To prevent wall slip,

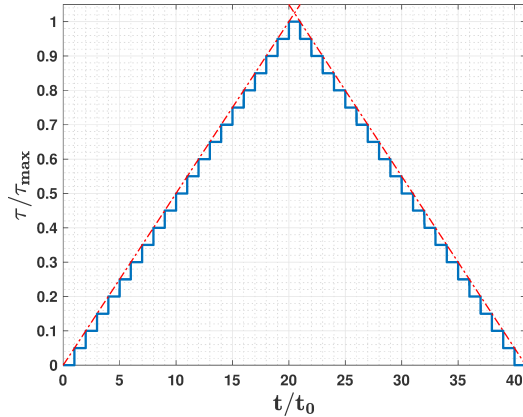


Figure 5: Schematic representation of the linear stepped stress ramp. For clarity of the presentation, we have chosen here $N = 20$ steps of each of the two branches of the ramp while during the experiments we report herein $N = 500$.

glass paper with an average roughness of $500 \mu m$ was glued on each plate. To account for the addition of the glass paper on the rotating plate of the device, the inertia of the device was recalibrated. The absence of any wall slip effect was verified by measuring flow curves in subsequent tests performed with several values of the gap and showing that all measurements perfectly overlap. To prevent the evaporation of the solvent during the rheological measurements a thin layer of commercial oil was added to the free meniscus of the sample.

Most of the rheological measurements were performed according to the following protocol. First, the sample was pre-sheared at a constant applied stress larger than the yield stress for $300 s$ and allowed to relax for another $300 s$. Then, to assess the rheological behaviour of the Carbopol gel in different deformation regimes, a commonly used rheological test consisting of loading/unloading the material according to an increasing/decreasing linear stress ramp was applied to a fluid sample, Fig. 5. For all the experiments reported herein, the maximum stress was chosen $\tau_{max} = 20 Pa$ (which is significantly larger than the yield stress $\tau_y \approx 8.9 Pa$) and the number of steps of each branch of the ramp was fixed $N = 500$. To test the role of the rate at which the material is loaded/unloaded, the duration of each step was t_0 was varied between $0.2 s$ and $2 s$. Through the rest of the manuscript t_0 will be referred to as the “characteristic forcing time”. We note that for large enough number of steps N the stepped ramp is well approximated by a continuous linear ramp $\tau = Bt$ with the slope $B = \frac{\tau_{max}}{Nt_0}$, the dashed lines in Fig. 5.

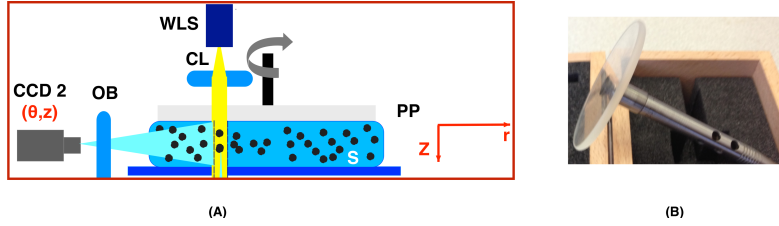


Figure 6: (a) Schematic representation (not in scale) of the micro-rheo-PIV system used to measure the dependence of the tangential velocity component at $r = 5R/6$ (R being the radius of the plate used during the rheological tests) on the vertical coordinate z . (b) Photograph of the serrated transparent disk used for the micro-rheo-PIV measurements.

In addition to the controlled stress ramps, we have monitored the response of the gel to steps in the rate of shear. To test the reproducibility and quantitatively assess the instrumental error, each rheological measurement was repeated three times with a fresh sample.

2.3. Micro-rheo digital particle image velocimetry observations of the rheometric flow

To get insights into the structure of the rheometric flow and check for the possibility of shear banding a home made micro-rheo PIV system schematically illustrated in Fig. 6 was used. For a detailed description of the experimental system and of the approach the reader is referred to Ref. [42]. It consists of parallel plate geometry equipped with a sandblasted glass plate (see panel (b) in Fig. 6)).

Whereas the optical transparency of the plate does not suffice for the visualisation of the flow, it is sufficient for the bulk illumination of the fluid by a white light source WS . The flow is visualised from the side through a hyper-zoom lens from the side using a digital camera (CCD). The measuring plane is orthogonal to the bottom plate of the rheometer. The size of the field of view is roughly $300\mu m \times 450\mu m$. The Carbopol gel is seeded with a small amount of polyamide spheres with an average diameter of $5\mu m$. Time series of velocity fields measured right below the top disk in a vertical plane are obtained from pairs of subsequent images using a Digital Particle Image Velocimetry (DPIV) tool implemented in the house under Matlab. The instrumental accuracy of the micro-DPIV measurements was 7% of the measured speed.

3. Results

3.1. Yielding of a Carbopol gel to stress revisited

None of the the three simple flows exemplified in Sec. 1.2 can be theoretically rationalised in the framework of a “*model*” yield stress material. This prompts us to revisit the yielding scenario of a Carbopol gel in a simple rheometric flow.

The “*model*” yield stress picture of a Carbopol gel summarised in Sec. 1.1 was challenged for the first time by Putz and Burghelea, [33]. The main approach in Ref. [33] was to perform controlled stress ramps for both increasing and decreasing values of the applied stresses according to the protocol schematically illustrated in Fig. 5 and described in Sec. 2.2. While the maximum stress during the ramp τ_{max} and the number N of steps of each branch were fixed, the characteristic forcing time t_0 was varied.

The limit of steady state forcing corresponds to large values of t_0 . We illustrate in Fig. 7 the dependence of the measured absolute value of the rate of shear $|\dot{\gamma}_0|$ on the normalised applied stress τ/τ_y for $t_0 = 1.5 s$. The yield stress τ_y was obtained via a classical Herschel-Bulkley fit, $\tau_y \approx 8.9 Pa$. The data set presented in Fig. 7 is the very same data set presented in Fig. 1 but only plotted on a log-log scale. Prior to discussing the main features of the solid-fluid transition it is worth noting that results qualitatively similar to that illustrated in Fig. 7 have been obtained using various rheometers, various concentrations of Carbopol, and at various temperatures [33, 44, 23, 32, 40, 8, 26]. More recently, a rheological hysteresis qualitatively similar to our result was observed by Divoux and coworkers, [19].

Several important features some of which are at odds with the “*model*” yield stress picture may be noticed in Fig. 7 :

1. For low values of the applied stress, a plateau of the shear rate is observed on both branches of the flow ramp. As the stress ramp was linear in time, such plateaus are the signature of an elastic solid behaviour. This can be easily demonstrated as follows. A plateau $\dot{\gamma} = \dot{\gamma}_0 = ct$ observed for low stresses during linearly increasing/decreasing stress ramp $\tau = Bt$ implies $\gamma = \dot{\gamma}_0 t = \frac{\tau \dot{\gamma}_0}{B}$ or $\tau = G\gamma$ with $G = \frac{B}{\dot{\gamma}_0}$ which is the Hooke’s law.
2. For high values of the applied stresses a fluid regime (**F**) that can be accurately described by the Herschel-Bulkley constitutive model (the full line) is observed.
3. In spite of the visual impression given by Fig. 1 which displays the very same data but plotted on a linear scale, the transition from the solid regime (**S**) to the fluid regime (**F**) is not direct (i.e. does not occur

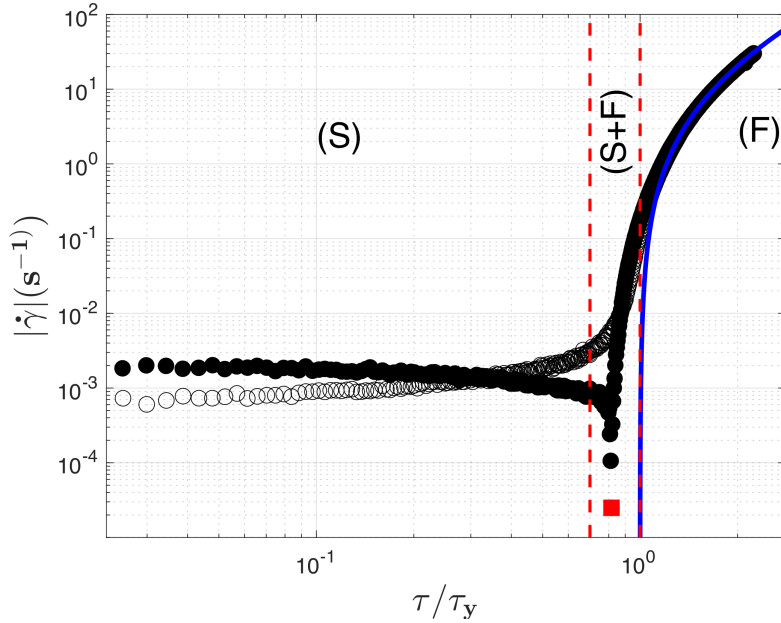


Figure 7: Dependence of the absolute value of the rate of shear $|\dot{\gamma}|$ on the reduced applied stress τ/τ_y measured for increasing (empty symbols) and decreasing (full symbols) imposed stresses. The stresses were varied linearly in time and the characteristic forcing time was $t_0 = 1.5$ s. The vertical dashed lines separate the three deformation regimes: **(S)** - solid, **(S+F)** - intermediate and **(F)** - fluid. The full square marks the point of elastic recoil (the rate of shear changes sign) systematically observed on the decreasing stress branch of the ramp. The full line is a fit by the Herschel-Bulkley model.

at a well defined value of the stress) but mediated by an intermediate deformation regime **(S+F)**.

4. With the exception of the fluid regime **(F)**, the measurements are not reproducible upon increasing/decreasing the applied stress and a clear rheological hysteresis is observed.
5. On the decreasing branch of the applied stresses, there exists a critical value of the applied stress $\tau_c/\tau_y \approx 0.8$ below which the shear rate changes sign (the spindle of the rheometer reverses its sense of rotation). This may be understood in terms of a recoil effect which is correlated to both the elasticity of the gel and the momentum of inertia of the plate geometry.

It is rather clear that the points (3 – 5) enumerated above are at odds with the “*model*” yield stress picture.

However, the measurements presented in Fig. 7 contain all the physical “*ingredients*” needed to phenomenologically understand the topology of the

flow fields observed during the sedimentation experiments illustrated in Fig. 2 and during the Landau-Levich experiment illustrated in Fig. 3.

The breakdown of the fore-aft symmetry of the flow pattern measured during the sedimentation experiment Fig. 2 may be related to the emergence of a rheological hysteresis observed upon increasing/decreasing stresses past the **(S+F)** deformation regime by simply noting that the material located in the fore region of the sphere is being progressively loaded while the material located in the aft region is being unloaded.

The emergence of the negative wake during both the sedimentation experiment Fig. 2 and the Landau-Levich experiment Fig. 3 may be directly related to the recoil effect observed during the unloading branch of the controlled stress ramp.

3.2. Visualisation of the Carbopol microstructure

Dinkgreve and coworkers pointed out that Carbopol gels behave as "model" yield stress materials if they are "properly" prepared, [16]. By "properly", the authors mean the gel is not over-stirred during the neutralisation phase of the preparation procedure and explain that the over-stirring would mechanically destroy the micro-structure even at a neutral pH which ultimately leads to a non-model rheological behaviour (e.g. emergence of stress overshoot during step-strain rheological tests, rheological hysteresis during increasing/decreasing ramps of stresses) and emergence of a negative wake during sedimentation experiments similar to those exemplified in Sec. 1.2.1. To support this statement, the authors present in Fig. 5 of their paper micrographs of a gently stirred (structured) Carbopol gel sample versus a strongly stirred (de-structured) Carbopol sample. The micrographs were obtained by adding molecular Rhodamine 6G (few drops of an aqueous solution of Rhodamine 6G with a concentration of $10^{-5}M$) to a 0.5% (*wt*) aqueous solution of Carbopol Ultrez U10.

To test whether the micro-structure of the Carbopol solution used in our rheological tests was mechanically damaged during preparation or not, we have carefully followed the procedure described in Ref. [16], added $10^{-5}M$ of molecular Rhodamine 6G to the Carbopol solution and attempted to visualise the microstructure by means of classical epi-fluorescent microscopy. The results of this attempt are summarised in Fig. 8.

In an acid state (just after the complete dissolution of the anhydrous Carbopol in deionised water) at $pH = 3$ a microstructure is clearly visible, panel (a) in Fig. 8. Upon neutralisation (at $pH \approx 7$) the microstructure is no longer visible, panel (b) in Fig. 8. A similar unsuccessful attempt of visualising the microstructure of a neutral Carbopol solution by simply

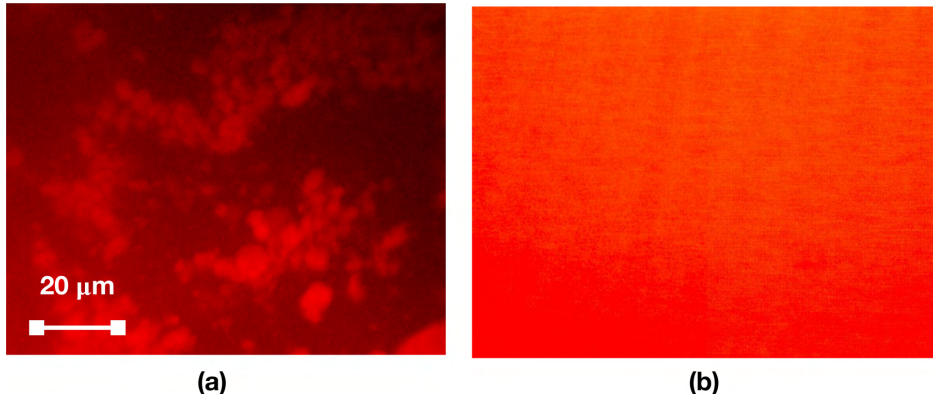


Figure 8: Fluorescent micro-graph of a 0.1% (wt) solution of Carbopol 980 containing a $10^{-5} M$ aqueous solution of molecular Rhodamine 6G at **(a)** $pH = 3$ (no measurable yield stress). **(b)** $pH = 7$ (measurable yield stress).

adding an ionic dye (Acrydine Orange) has been reported by Gutowski and coworkers, [24].

The differences in the visualization of Carbopol by Rhodamine 6G in different environments can be explained in terms of basic organic chemistry as follows. In acid environment at $pH = 3$ Carbopol is in a dissociated state and the Rhodamine is bound to the Carbopol by non-covalent interactions such as ionic bonds. To help understanding this point, we illustrate in Fig. 9(a) the molecular structure of Rhodamine 6G. However, in neutral conditions at $pH = 7$ the carboxylic groups of Carbopol which allow this ionic bonding are neutralised. Thus, Rhodamine 6G does not interact preferentially with Carbopol and it is homogeneously distributed in the solution (the Rhodamine has a low molar mass, so it diffuses easily in the solvent), which leads to non-specific visualisation of the system 8(b).

To visualise the microstructure of the Carbopol, we have elaborated a more sophisticated chemical protocol able to covalently bind molecules of Rhodamine *B* to the backbone of the poly-acrylic acid. To help understanding this point, we illustrate in Fig. 9(b) the molecular structure of Rhodamine *B*. As compared to the ionic bonding attempted by Dingre and coworkers in Ref. [16], the net advantage of the covalent bonding comes from the fact that the covalent bonds are not destroyed during the neutralisation step of the Carbopol solution.

The Carbopol with covalently bound Rhodamine *B* was prepared by three-step synthesis. In the first step the Rhodamine *B* was esterified with ethylene glycol providing 2-hydroxyethyl ester, which was in the second step transformed to 2-bromoethyl ester. In the last step the bromine-modified

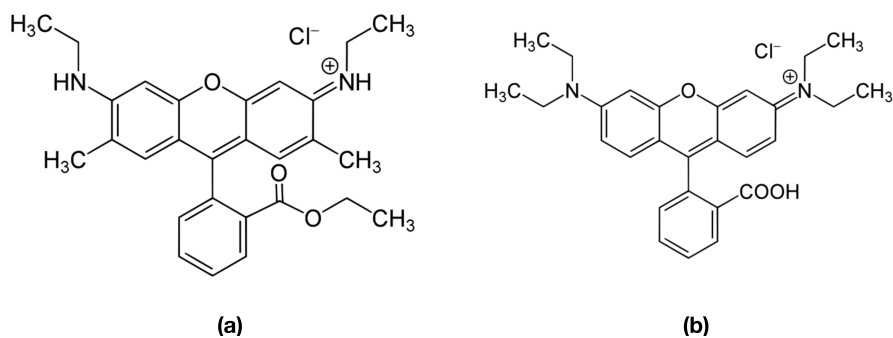


Figure 9: (a) Molecular structure of Rhodamine 6G used by Dinkgreve and coworkers in Ref. [16]. (b) Molecular structure of Rhodamine B used in the present study.

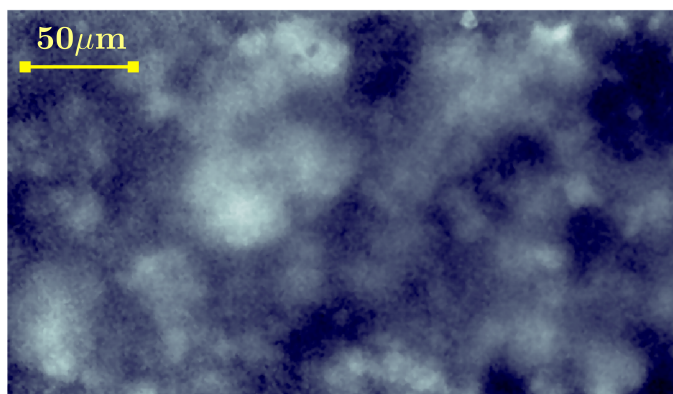


Figure 10: Micrograph of the neutral Carbopol gel covalently labelled with Rhodamine B (see text for description). The bright details of the micrograph refer to the Carbopol particles while the dark details refer to the aqueous solvent.

Rhodamine B was grafted on Carbopol under basic conditions. The detailed description of the synthesis protocol goes beyond the scope of this contribution and it will be given in a subsequent paper.

A micrograph of the covalently labelled Carbopol gel is illustrated in Fig. 10. The bright details in this image refer to Carbopol particles while the dark regions refer to the solvent (deionised water). It is clear from Fig. 10 that the gel is highly structured and the average size of the micro-structure is of the order of 50 μm. This characteristic size is consistent with the results reported in Refs. [29, 28].

3.3. On the physical reasons behind the emergence of the rheological hysteresis during the loading/unloading of the Carbopol sample

After being reassured that the rheological hysteresis observed upon loading/unloading of the Carbopol gel (Fig. 7) it is not related to a mechanical damage of the micro-structure, we discuss in the following several possible physical reasons behind this observation. A first important contribution to the emergence of the rheological hysteresis relates to the elastic effects within the regimes **(S)** and **(S+F)**. As shown in Fig. 7 and highlighted in Sec. 3.1 elasticity manifests through the emergence of a plateau of shear rates in the **(S)** regime and through an elastic recoil on the unloading branch. These elastic effects coupled to an unsteady loading/unloading of the sample may phenomenologically lead to the observation of a rheological hysteresis.

Another possible physical reason responsible for the emergence of a rheological hysteresis relates to the presence of shear banding in the flow. Indeed, shear banding has been observed experimentally with Carbopol gels, [20]. To test whether shear banding occurred during the rheological measurements, we resort to the micro-rheo-DPIV technique described in Sec. 2.3.

Using this setup, 500 individual flow fields were measured in the plane $z-r$ within the sample at the radial position $r = 5R/6$ (R being the radius of the top glass made disk). The stress was chosen such as the system would be within the regime **S+F**. A time averaged flow field is shown in Fig. 11(a) and dependence of the azimuthal velocity component U on the vertical coordinate is shown in Fig. 11(b). The error bars defined by the root mean square deviation of the measured velocity computed with 500 instantaneous velocity fields does not exceed 7% of the measured value, Fig. 11(b). Two distinct flow regions can be seen in Fig. 11(b). For $z < 150\mu m$ the velocity profile is flat (meaning $\frac{\partial U}{\partial z}$) which is consistent with the presence of a solid plug located near the top disk. For $z > 150\mu m$ the slope of the dependence $U = U(z)$ is no longer null: the material flows.

Thus, we may conclude that shear banding was present during the rheological measurements which, according to Divoux and coworkers, contributes to the emergence of the rheological hysteresis [19]. To conclude this part, the emergence of hysteresis may be phenomenologically triggered by several combined effects: elasticity, unsteady loading/unloading and shear banding. Through the rest of the manuscript we restrict our discussion to the first two effects. A systematic discussion of the shear banding and an analysis of the space-time dynamics of the micro-rheo-DPIV measured flow fields goes beyond the scope of the present contribution and will be published elsewhere.

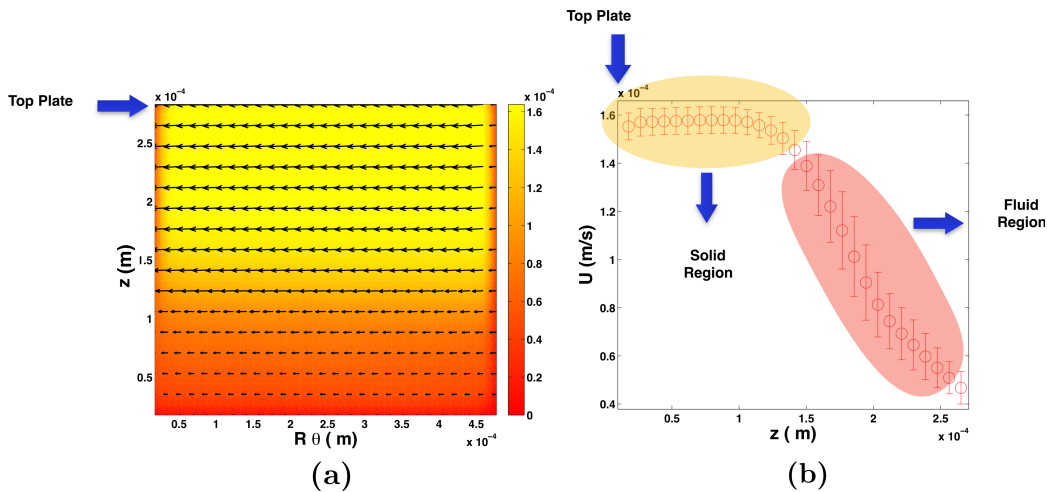


Figure 11: (a) Time averaged (over 500 instantaneous velocity fields) velocity field. The false colour map refers to the magnitude of the velocity. (b) Dependence of the time averaged azimuthal velocity component U on the vertical coordinate z . The error bars are defined by the root mean square deviation obtained by performing a statistical analysis over 500 instantaneous flow fields and do not exceed 7% of the measured value.

3.4. Role of the rate of the forcing on the dynamics of the solid-fluid transition

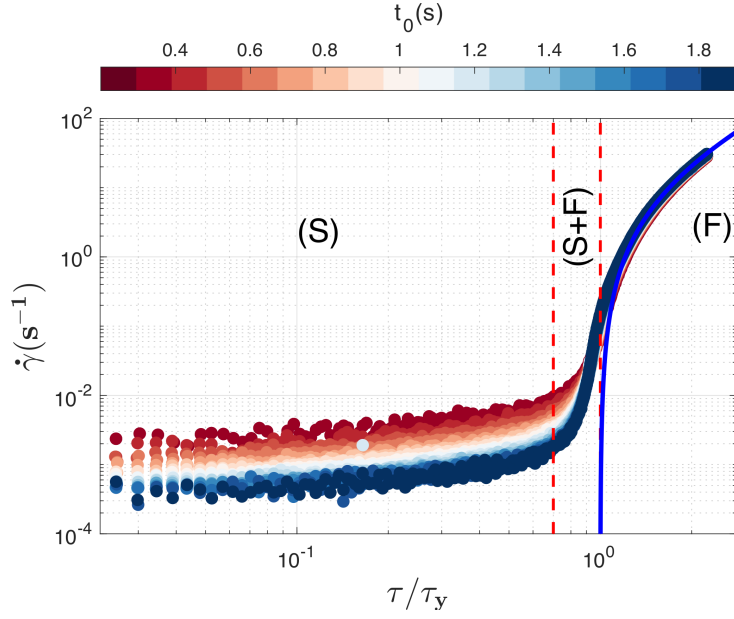
We address in the following the question of how the rate at which the material is loaded/unloaded influences the rheological measurements. A quantitative measure of rate of the loading/unloading process is given by the characteristic forcing time t_0 . The choice of monitoring the response of the Carbopol gel during an unsteady loading/unloading process rather than a steady state forcing scheme is clearly motivated by the "simple" flows illustrated in Sec. 1.2.

To understand this we perform controlled stress ramps similar to the one illustrated in Fig. 7 for various values of the characteristic forcing time (the time per stress step) t_0 , Fig. 12.

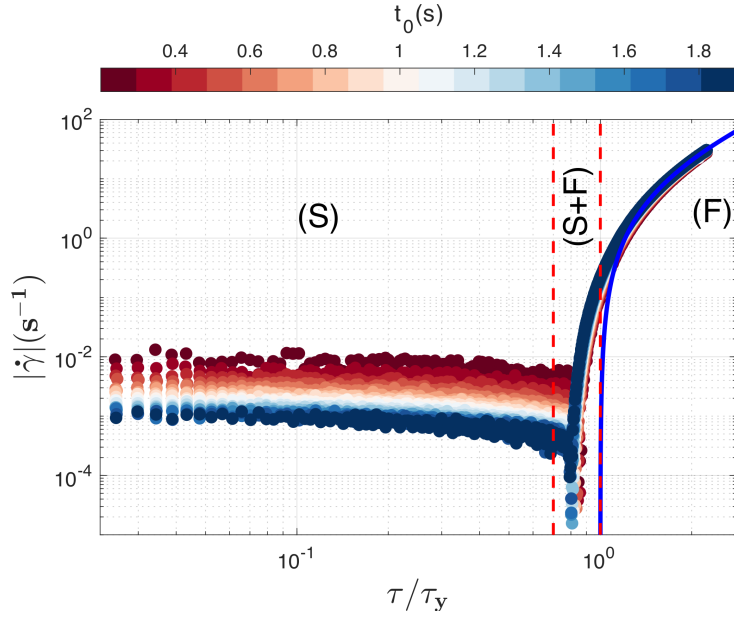
For clarity of the presentation, we present the data acquired on the increasing branch of the stress ramp in Fig. 12(a) and the data acquired on the decreasing branch of the ramp in Fig. 12(b).

Regardless the branch of the ramp, a clear dependence of the measured shear rate on the characteristic forcing time t_0 is observed within the solid deformation regime (**S**) and within the intermediate regime (**S+F**). On both branches, for low values of the imposed stress, a plateau of the rate of shear is observed.

As explained in Sec. 3.1 the emergence of these plateaus is an indicator that, at low applied stresses, the material follows Hooke's law.



(a)



(b)

Figure 12: 12(a) Dependence of the rate of strain $\dot{\gamma}$ on the imposed stress measured on the increasing branch of the stress ramp for various values of the characteristic forcing time t_0 . 12(b) Dependence of the absolute value of the rate of strain $|\dot{\gamma}|$ on the imposed stress measured on the decreasing branch of the stress ramp for various values of the characteristic forcing time t_0 . In both panels, the top colour bar maps the value of t_0 . The vertical dashed lines separate the solid deformation regime **(S)** the intermediate regime **(S+F)** and the fluid deformation regime **(F)**. The full line is a nonlinear fit by the Herschel-Bulkley model.

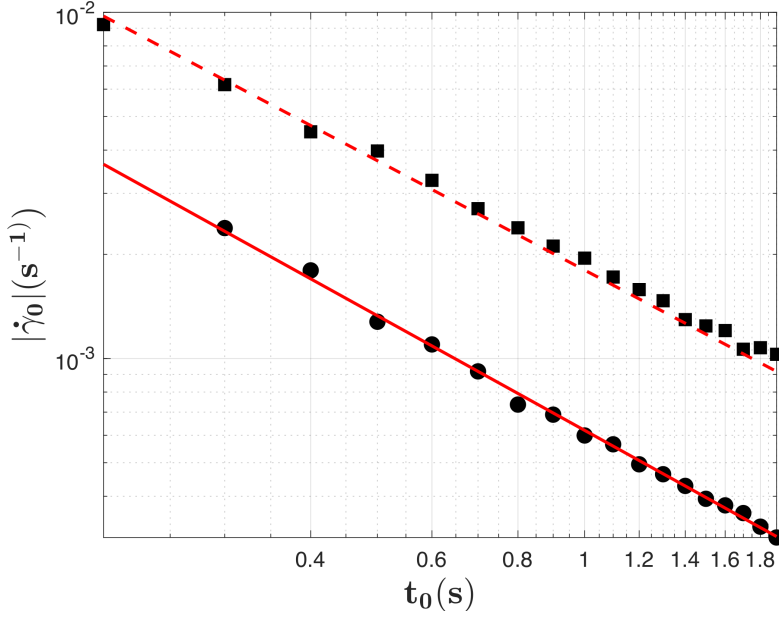


Figure 13: Dependence of the shear rate plateau value $|\dot{\gamma}_0|$ on the characteristic forcing time t_0 measured on the increasing ramp (circles) and the decreasing branch of the stress ramp (squares). The full line is a power law fit, $\dot{\gamma}_0 = 10^{-4} + 7 \cdot 10^{-4} t_0^{-1.06}$. The dashed line is a power law fit, $\dot{\gamma}_0 = 10^{-4} + 0.0018 t_0^{-1.05}$.

To get further insights into this, we plot in Fig. 13 the dependence of the value of the shear rate plateau observed at low shear stresses $\dot{\gamma}_0$ on the characteristic forcing time t_0 measured on both the increasing (circles) and decreasing (squares) branch of the stress ramp.

On both branches of the stress ramp, a power law scaling of the low stress shear rate plateau is observed, $\dot{\gamma}_0^{u,d} \propto t_0^{-1}$ - the full/dashed lines in Fig. 13. The low applied stress plateau values of the rate of shear measured on the increasing branch of the ramp are systematically smaller than the values measured on the decreasing branch, $\dot{\gamma}_0^u < \dot{\gamma}_0^d$ which implies $G^u > G^d$. This may be understood as follows. At the end of the unloading process (the decreasing branch of the stress ramp), the material has accumulated a long de-structuring history and cannot return to the initial solid state characterised by G^u but to a “softer” solid state characterised by $G^d < G^u$. The elastic moduli $G^{u,d}$ may be estimated using the slope B of the stress ramp $G^{u,d} = \frac{B}{\dot{\gamma}_0^{u,d}} = \frac{\tau_{max}}{N} \frac{1}{t_0 \dot{\gamma}_0^{u,d}}$ which using the power law fit results shown in Fig. 13, leads to $G^u \approx 57 Pa$ and $G^d \approx 22 Pa$.

A measure of the deficit of the deformation power per unit volume of material is given by the area of the hysteresis observed in Fig.7 defined as:

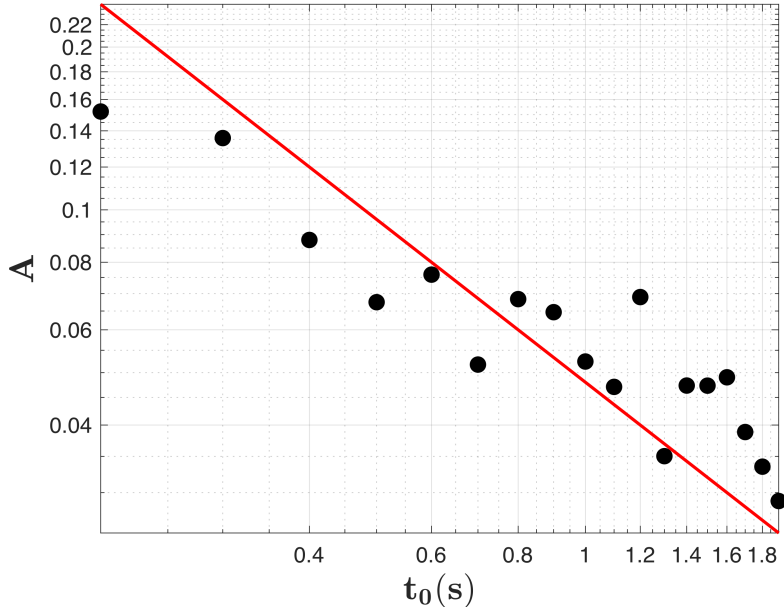


Figure 14: Dependence of the magnitude of the rheological hysteresis on the characteristic forcing time t_0 . The full line is a guide for the eye, $A \propto 1/t_0$.

$$A = \frac{1}{\tau_y} \left| \int_0^{\tau_{max}/\tau_y} \dot{\gamma}^u d\tau^u - \int_0^{\tau_{max}/\tau_y} |\dot{\gamma}^d| d\tau^d \right| \quad (1)$$

The dependence of the magnitude of the rheological hysteresis A on the characteristic forcing time t_0 is shown in Fig. 14. As the characteristic forcing time is increased, the magnitude of the rheological hysteresis decays as a power law, $A \propto t_0^{-1}$ - the full line in Fig. 14. This means that, in the asymptotic limit of a steady state forcing the deformation states are practically reversible upon increasing/decreasing stresses and the Carbopol gel tends to behave as a “*model*” yield stress material. A qualitatively similar power law decay of the area of the hysteresis was reported by Divoux and coworkers, [19].

3.5. On modelling the yielding transition in a Carbopol gel: how simple a rheological model can get (and yet remain meaningful)?

We aim in this section at finding a minimalistic rheological model able to describe the yielding behaviour of a Carbopol gel presented in Secs. 3.1, 3.4 and illustrated in Figs. 7, 12. Several phenomenological macroscopic models have been proposed [21, 36, 35, 37, 9, 10, 38, 33, 12, 13, 14, 15, 7] which have

a general form:

$$\frac{d\Phi(t)}{dt} = F_1 [\Phi(t), \tau(t), C_1, C_2, \dots, C_m] \quad (2)$$

The distinctive feature of these models is that they describe the temporal evolution of a micro-structural parameter $\Phi(t)$ as a function of the applied stress and a number of parameters C_1, \dots, C_m . Part of these parameters describe the kinetics of the destruction/re-structuration of the material and are difficult (or impossible!) to measure. The rest of the parameters describe the rheological behaviour of the material (e.g. yield stress, consistency, power law index, elastic modulus) which may be measured via adequate macroscopic rheological tests (flow ramps, oscillatory measurements, creep/relaxation tests etc.). The functional dependence F_1 is often chosen on a phenomenological (and semi-empirical) basis rather than derived from first principles. The micro-structural equation 2 needs to be complemented by a constitutive relationship which takes the general form:

$$\tau(t) = F_2 \left[\Phi(t), \frac{d\tau(t)}{dt}, A_1, A_2, \dots, A_m \right] \quad (3)$$

where the material constants A_1, A_2, \dots, A_m reflect the rheological behaviour of the material. A choice of the functional dependencies F_1 and F_2 that is suitable for modelling the response of a Carbopol gel to stress must satisfy (at least) two fundamentals requirements:

1. In the asymptotic limit of very small applied stresses, Eq. 3 should reduce to Hooke's law: $\tau = G\gamma$.
2. For applied stresses significantly larger than the the yield stress one needs to recover the Herschel-Bulkley constitutive relationship: $\tau = \tau_y + K|\dot{\gamma}|^n$.

Besides these basic requirements there exist at least two important requirements a comprehensive micro-structural model should meet. First, a micro-structural model needs to be thermodynamically validated, [41, 14]. This requirement is more difficult to fulfil particularly when the functional dependence F_1 is prescribed on a phenomenological (semi-empirical basis). An alternative way of prescribing a thermodynamically validated evolution equation for the microstructure has been recently proposed using a Gibbs field microscopic yielding picture similar to the magnetisation of a lattice of atomic spins and built upon fundamental principles of *Statistical Physics*, [39, 40, 8].

Second, such models should also be able to capture the shear banding phenomenon which is often observed during the yielding process, [17, 19]. Obviously, this task is impossible to achieve by a scalar model. Through the

reminder of this section we will not discuss the thermodynamic aspect and the shear banding but focus on a significantly more modest quest: identify a minimalistic scalar model that satisfies the two base requirements afore stated and is able to accurately describe the experimentally observed yielding scenario of a Carbopol gel.

3.5.1. Applicability of the model proposed in Ref. [9] in describing the rheological response of a Carbopol gel

One of the simplest micro-structural models was proposed by Coussot and coworkers, [9]. The time derivative of the structural parameter depends linearly on the shear rate according to:

$$\frac{d\Phi(t)}{dt} = \frac{1}{\lambda} - \alpha\Phi(t)\dot{\gamma}(t) \quad (4)$$

The micro-structural equation has a single steady state solution, $\Phi_{SS} = \frac{1}{\lambda\alpha\dot{\gamma}}$. The viscosity of the material is directly related to the micro-structural parameter ¹:

$$\eta(t) = \eta_0 [1 + \beta\Phi(t)^n] \quad (5)$$

An important claim made in Ref. [16] is that, when over-stirred during preparation, the Carbopol gel becomes weakly thixotropic and its rheological behaviour can be described by the model proposed in Ref. [9]. This is clearly illustrated in Fig. 7 of Ref. [16] which presents measurements of a flow curve for an increasing/decreasing ramp in shear rates together with an excellent fit using the model proposed in Ref. [9]. During their tests the duration of each step in the shear rate was $t_0 = 10s$ (according to insert of Fig. 7 of Ref. [16]). To fit their data, the authors set $\beta = 1$, $n = 2$ (not to be confused with the power law index in the Herschel-Bulkley law), $\lambda = 10s$ and α obtained from the yield stress via $\alpha = \frac{2\eta_0\beta}{\lambda\tau_y}$.

Prior to assessing this claim and attempting to describe the yielding behaviour of the Carbopol gel used in this study with this model we make several rather obvious remarks:

1. In the limit of high applied shear rates when the structural parameter Φ is expected to vanish (if one assumes that the microstructure will be entirely destroyed far above the yield point) the model described above predicts a Newtonian behaviour, $\lim_{\Phi \rightarrow 0} \eta(\Phi) = \eta_0$. This is somewhat at odds with the universally recognised fact that Carbopol gels sheared

¹The equation used in Ref. [16] was $\eta(t) = \eta_0 [1 + \beta\Phi(t)]^n$, but, as the authors make reference to the first paper that introduces the model (Ref. [9]) we believe this was merely a typo.

at rates far above the yield point exhibit a shear thinning behaviour, $\eta \propto \dot{\gamma}^{n-1}$ (with $n \in (0, 1)$) and a high shear rate Newtonian plateau has been never observed experimentally. Thus, the only way of recovering a shear thinning response with this model is to assume that even far beyond the yield point the structural parameter remains strictly positive, $\Phi > 0$. Certainly, such an assumption is difficult to justify on either a theoretical or an experimental basis for the case of a Carbopol gel.

2. Corresponding to a linearly increasing (with time) and continuous ramp in shear rates $\dot{\gamma}(t) = At$, there exists an analytical solution for the structural parameter:

$$\Phi(t) = \frac{e^{-\frac{1}{2}A\alpha t^2} \left[\sqrt{2\pi} \text{Erfi} \left(\frac{\sqrt{A\alpha}t}{\sqrt{2}} \right) + 2\Phi(0)\lambda\sqrt{A\alpha} \right]}{2\sqrt{A\alpha}\lambda} \quad (6)$$

The analytical solution of Eq. 6 is generally non monotonic: prior to decaying to zero as t increases it passes through a local maximum. This means that, prior to yielding, the material first ages to a state $\Phi_m = \max\{\Phi(t)\} > \Phi(0)$ which depends strongly on the choice of the initial condition $\Phi(0)$. Except for the data presented by Dinkgreve and coworkers in Fig. 7 of Ref. [16] we are not aware of any other independent experimental observation of ageing of a Carbopol gel prior to yielding within time windows of order of tens of seconds during a controlled rate ramp.

To gain further insights into applicability of this model in describing the flow curves of a Carbopol gel and compare our findings with the data published in Fig. 7 of Ref. [16] we consider an increasing/decreasing stepped ramp in the rate of shear in the form:

$$\dot{\gamma}(t) = \dot{\gamma}_{max} \frac{-2N + 1 + \sum_{k=0, t_0}^N H(t - k) + \sum_{k=N+1, t_0}^{2N} H(k - t)}{N} \quad (7)$$

Here H stands for the Heaviside step function, t_0 is the duration of each step of the ramp and $T_{max} = N t_0$ is the total duration of the loading/unloading branches. To avoid numerical issues while solving the coupled equations Eqs. 4, 5 we approximate the Heaviside functions involved in the summations in Eq. 7 as $H(t) \approx \frac{1}{2} \left[1 + \tanh \left(\frac{t}{t_s} \right) \right]$ with t_s being a small smoothing factor.

As in Ref. [16] we choose $t_0 = 10s$, $\lambda = 10 s$, $\eta_0 = 0.1 mPas$, $\beta = 1$, $n = 2$ and compute the parameter α using the yield stress, $\alpha = 0.0022$. The numerical solution $\Phi(t)$ of the Eq. 4 is computed using the Matlab function

ode23s. Last, we compute the viscosity using the numerical solution of the structural parameter according to Eq. 5.

The numerical solutions of the model obtained for six different values of the initial condition $\Phi(0)$ are shown in Fig. 15. In each of the panels of Fig. 15 the colours map the value of the initial condition $\Phi(0)$ (see the top colour bars), the full lines and symbols refer to the increasing branch of the shear rate ramp while the dash-dotted lines and the empty symbols refer to the decreasing branch of the ramp.

As one would expect from the analytical solution expressed by Eq. 6, regardless the value of the initial condition $\Phi(0)$, the structural parameter first increases when the shear rate increases up to a maximal value and the magnitude and position of the local maximum depends strongly on $\Phi(0)$, Fig. 15(a). Corresponding to large applied shear rates $\dot{\gamma} \geq \dot{\gamma}_c \approx 50 \text{ s}^{-1}$, the numerical solutions computed for various initial conditions overlap. The numerical solutions of the structural parameter computed for various $\Phi(0)$ on the decreasing branch of the shear rate ramp are monotonic and overlap - the dash-dotted lines in Fig. 15(a).

The local maxima of the structural parameter observed on the increasing branch of the ramp result in local maxima of both the reduced stress τ/τ_y Fig. 15(b) and of the viscosity, Fig. 15(c). Past these maxima the reduced stresses decrease steeply up to $\dot{\gamma} \approx \dot{\gamma}_c$ and then increase linearly which is consistent with a nearly Newtonian rheological behaviour (see the dashed line of unitary slope in Fig. 15(b)). This steep decrease of the stresses past the local maxima translates into a seemingly shear thinning behaviour of the viscosity solutions Fig. 15(c). At a closer look, however, the slopes of the decay of the viscosity in this range of shear rates are systematically steeper than -1 (the dashed line in Fig. 15(c)) and increase as the initial condition $\Phi(0)$ increases. This simply means that this viscosity decay can not be intrinsically connected to a shear thinning behaviour ($\eta \propto \dot{\gamma}^{n-1}$ with $n \in (0,1)$) and it solely emerges as a result of an arbitrary choice of the initial condition $\Phi(0)$.

Yet the biggest surprise comes when plotting the numerical solutions of the viscosity against the reduced stress, Fig. 15(d): all the numerically obtained dependencies are multi-valued! We are not aware of any published rheological data obtained with a Carbopol gel showing two distinct values of the viscosity for the same applied stress.

To conclude the analysis of the applicability of the model proposed in Ref. [9] in describing the yielding behaviour of a Carbopol gel, the following points may be summarised:

1. In the asymptotic limit of small applied shear rates the model can not

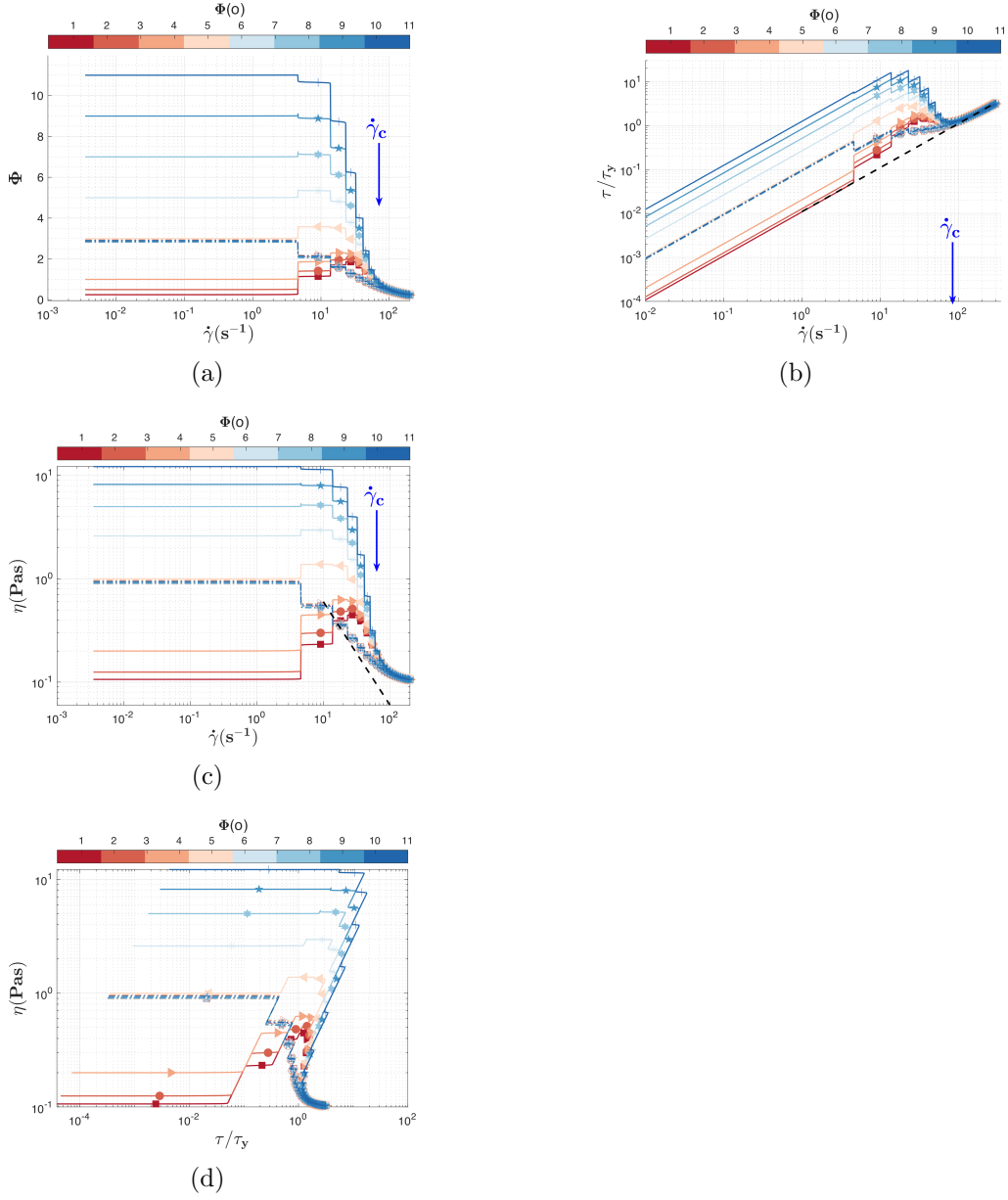


Figure 15: Response of the model proposed in Ref. [9] to a ramp in the shear rate (see text for details): (a) Dependence of the micro-structural parameter Φ on the imposed shear rate $\dot{\gamma}$. (b) Dependence of the reduced stress τ/τ_y on the imposed shear rate $\dot{\gamma}$. The dashed line is a guide for the eye, $\tau/\tau_y \propto \dot{\gamma}$ which is the Newtonian asymptotic limit of the model. (c) Dependence of the viscosity η on the imposed shear rate $\dot{\gamma}$. The dashed line is a guide for the eye, $\eta \propto \dot{\gamma}^{-1}$. (d) Dependence of the viscosity η on the reduced stress τ/τ_y . The various colours in each panel refer to the initial condition of the micro-structural parameter $\Phi(0)$ mapped onto the top colour-bar. The full lines and the full symbols in each panel refer to the increasing branch of the ramp while the dashed-dotted lines refer to the decreasing branch of the ramp.

describe an elastic solid rheological behaviour as observed in Fig. 12. In the limit of large applied shear rates, one can not recover a true shear thinning behaviour $\tau \propto \dot{\gamma}^n$ with $n \in (0, 1)$ as one would typically expect from a Carbopol gel in a fluid state.

2. Although a power law decay of the viscosity may be observed within a limited range of shear rates (prior to yielding), this decay is inconsistent with a true shear thinning behaviour because it is too steep even for the smallest initial value $\Phi(0)$ explored.
3. This model predicts a non monotonic increase of the stress with the rate of shear. Apart from the data published in Fig. 7 of Ref. [16] we are not aware of any other measurements performed with a Carbopol gel that reveal such a behaviour.
4. When plotted against the stress, the numerical solutions of the viscosity are multivalued which is obviously unphysical and has never been observed for a Carbopol gel.

Thus, the overall conclusion of this section is that, contrarily to what is claimed in Ref. [16], the model proposed in Ref. [9] is unable to accurately describe the yielding behaviour of a Carbopol gel subjected to a stepped ramp of shear rates.

3.5.2. Applicability of the model proposed in Ref. [33] in describing the rheological response of a Carbopol gel

As it is clear from the arguments given in Sec. 3.5.1 that the model proposed in Ref. [9] can not describe the yielding behaviour of a Carbopol gel we now turn our attention to another micro-structural model proposed in Ref. [33] and test its applicability in describing the rheological behaviour of a Carbopol gel detailed in Sec. 3.1.

According to Ref. [33] the evolution equation for the structural parameter Φ depends on the imposed stress τ according to:

$$\begin{aligned} \frac{d}{dt}\Phi(t) &= k_r \left[1 - \tanh\left(\frac{\tau - \tau_y}{w}\right) \right] \Phi(t)(1 - \Phi(t)) \\ &- k_d \left[1 + \tanh\left(\frac{\tau - \tau_y}{w}\right) \right] \Phi(t) + \delta. \end{aligned} \quad (8)$$

where k_r is the rate of recombination of micro-structural units, k_d is the rate of destruction of the solid phase, τ_y is the yield stress w is a constant that controls how steep the change in the microstructure from solid to fluid and fluid to solid is and δ is a small term accounting for the thermal noise. Unlike the micro-structural model proposed in Ref. [9], the evolution equation Eq.

8 has two steady state solutions which allows in principle bistability and the emergence of a genuine rheological hysteresis when the material is loaded and then unloaded, [33].

As a constitutive relationship one may consider a thixo-elastic Maxwell model similar to a number of micro-structural models proposed by Quemada, [36, 35, 37]:

$$\frac{\eta(\dot{\gamma})}{G} \Phi \frac{d\tau}{dt} + \tau = \eta(\dot{\gamma}) \dot{\gamma} \quad (9)$$

where G is the elastic modulus, $\dot{\gamma}$ the rate of shear and $\eta(\dot{\gamma}) = K\dot{\gamma}^{n-1} + \tau_y \frac{1-e^{-m|\dot{\gamma}|}}{|\dot{\gamma}|}$ is a Papanastasiou regularised Herschel-Bulkley viscosity function.

It is rather trivial to note that the asymptotic behaviour of the constitutive relationship given by Eq. 9 is fully consistent with the experimentally observed rheological behaviour of a Carbopol gel illustrated in Figs. 7, 12 and discussed in Sec. 3.1. For $\tau/\tau_y \rightarrow 0$ one obtains $\Phi \rightarrow 1$ and Eq. 9 reduces to Hooke's law: $\tau = G\dot{\gamma}$. In the asymptotic limit of large applied stresses $\tau/\tau_y > 1$ the entire material is fluidised $\Phi \rightarrow 0$ and Eq. 9 reduces to the Herschel-Bulkley law (or its regularised variant): $\tau = \tau_y + K|\dot{\gamma}|^{n-1}$.

To test the ability of this model to describe the yielding behaviour of a Carbopol gel, we consider an increasing/decreasing ramp of the applied stresses in the form:

$$\tau(t) = \tau_{max} \frac{-2N + 1 + \sum_{k=0, t_0}^N H(t - k) + \sum_{k=N+1, t_0}^{2N} H(k - t)}{N} \quad (10)$$

To describe the measurements presented in Fig. 7, we chose $\tau_{max} = 20Pa$, $t_0 = 1.5 s$ and $N = 500$. Corresponding to the forcing scheme described by Eq. 10, we find the values of the model parameters such as the numerical solution of the system of ordinary differential equations formed by Eqs. 8 and 9 matches the best the measurements presented in Fig.7.

In order to do so we have written a nested function program in Matlab. The main function uses the built-in function *lsqnonlin* in Matlab which solves nonlinear least-squares data fitting problems using a trust-region-reflective algorithm. As input we provide an initial guess for the parameters vector, the target data (see the symbols in Fig. 7) and a function which first solves the Eq. 8 for Φ using the built-in function *ode15s* in Matlab and then solves the constitutive relation defined by Eq. 9 for $\dot{\gamma}$ using the built-in function *fzero* in Matlab. The output of the main function is a vector with the optimal parameter values. We note that the increasing/decreasing branches of the flow ramp were fitted separately in order to properly capture the hysteresis behaviour visible in Fig. 7 within the **(S)** and **(S+F)** deformation regimes. The best fitting functions for the dependence of the rate of strain $|\dot{\gamma}|$ on the

applied stress τ/τ_y obtained according to this fitting/optimisation procedure are shown in Fig. 16(b) as full lines. The corresponding numerical solution of the micro-structural parameter Φ is shown in Fig. 16(a). It is clear from Fig. 16 that all the main features observed during the rheological tests and detailed in Sec. 3.1 are accurately described by the model.

A classical manifestation of elastic behaviour relates to the emergence of a stress overshoot during a rheological test consisting of a step in the rate of strain, $\dot{\gamma}(t) = H(t)\dot{\gamma}_{max}$. A systematic description of the stress overshoot observed with a Carbopol gel sample subjected to a step in the rate of strain was performed by Divoux and coworkers, [18].

On the other hand, Dinkgreve and coworkers show in Ref. [16] that an overshoot behaviour is solely observed with over-stirred samples which experienced a micro-structural damage, Fig. 3 therein.

We illustrate in Fig. 17 a clear overshoot behaviour observed for several imposed rates of strain $\dot{\gamma}_{max}$ which is fully consistent with the findings of Divoux and coworkers. Bearing in mind that the Carbopol sample used in this study did not undergo any micro-structural damage and contrarily to the claim made in Ref. [16] we conclude that the overshoot behaviour in our case is an intrinsic feature of the Carbopol gel which emerges from its elastic solid behaviour prior to yielding.

On a physical modelling side, the model proposed in Ref. [9] and discussed in Sec. 3.5.1 is clearly unable to predict an overshoot behaviour first and foremost because it lacks any elasticity. Therefore, we investigate in the following the ability of the model proposed in Ref. [33] to predict such behaviour. To do so, we have solved numerically the Eqs. 8 and 9 with a shear rate prescribed as $\dot{\gamma} = H(t)\dot{\gamma}_{max}$. To account for the mechanical inertia of the top disk of the rheometer we have followed Ref. [3] and added a source term in the right hand side of Eq. 9 as a single fit parameter². This inertial contribution should not be confused with the fluid inertia which was negligible for all the flows discussed through the manuscript. The rest of the parameters of the model were set to the same values obtained while fitting the dependence of the rate of strain on the applied stress shown in Fig. 16.

The result of fitting the stress overshoot data is shown in Fig. 17 as full lines. We may conclude that, in spite its simplicity, the model proposed in Ref. [33] is able to capture the stress overshoot phenomenon reasonably well.

²Such a correction was not needed while fitting the flow curve data because the increments in the rate of shear were small.

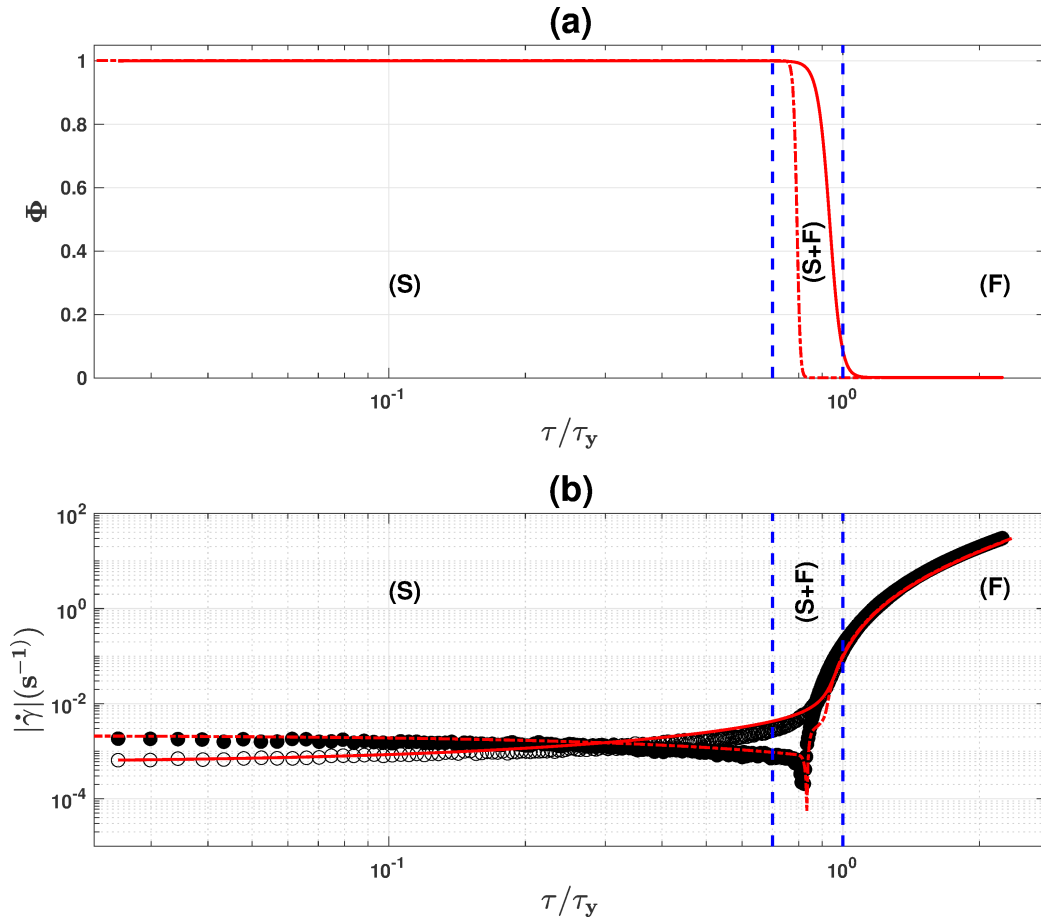


Figure 16: **(a)** Dependence of the structural parameter Φ on the applied stress obtained by solving numerically the elasto-viscoplastic model proposed by Putz and Burghelca, [33] for an increasing/decreasing stress ramp with $\tau_{max} = 20Pa$ and $t_0 = 1.5 s$. **(b)** Best fit of the dependence of the shear rate $|\dot{\gamma}|$ on the reduced applied stress τ/τ_y . In both panels the full/dash-dotted lines refer to the the increasing/decreasing branch of the linear stress ramp.

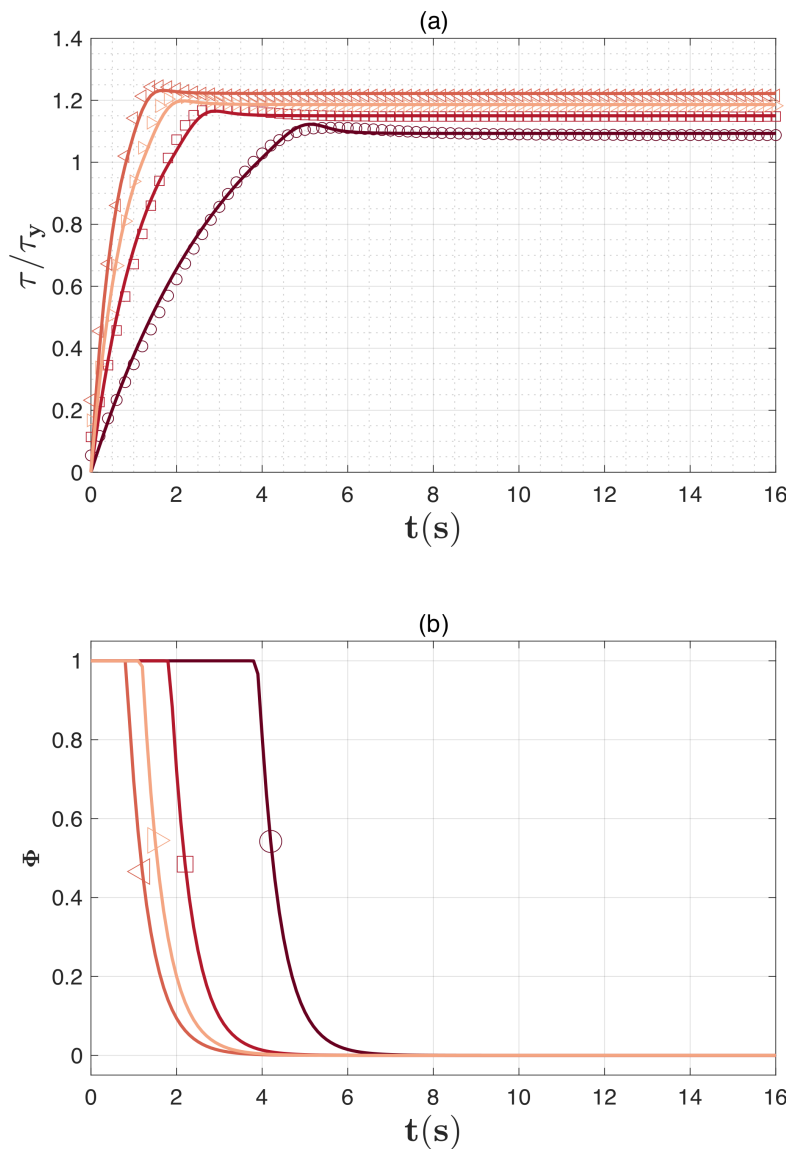


Figure 17: Stress overshoot observed during a step in the rate of shear $\dot{\gamma}(t) = H(t)\dot{\gamma}_{max}$: **(a)** Time dependence of the reduced stress τ/τ_y . The full lines are the numerical solutions of the model proposed in Ref. [33]. **(b)** Time dependence of structural parameter Φ . In both panels the symbols are: circles - $\dot{\gamma}_{max} = 0.5s^{-1}$, squares - $\dot{\gamma}_{max} = 1.5s^{-1}$, right triangles - $\dot{\gamma}_{max} = 2s^{-1}$, left triangles - $\dot{\gamma}_{max} = 3s^{-1}$.

4. Conclusions, outlook

The question regarding the nature of Carbopol gels subjected to stress (“*model*”, weakly thixotropic or time dependent yield stress materials) is addressed. After clarifying what is commonly understood by the “*model*” yield stress material picture of a Carbopol gel in Sec. 1.1, three examples of simple hydrodynamic experiments all at odds with this picture are detailed in Sec. 1.2: the low Reynolds number sedimentation of a spherical object in a Carbopol gel (Fig. 2), the Landau-Levich experiment (Fig. 3) and the emergence of thermo-convective instabilities within a Carbopol gel heated from below (Fig. 4).

By revisiting the rheological behaviour of a Carbopol gel in Sec. 3.1, a yielding behaviour strikingly different from that of a “*model*” yield stress material is revealed, Fig. 7. First, the transition from a solid regime (**S**) to a fluid regime (**F**) is not direct but mediated by an intermediate deformation regime (**S+F**) where solid and fluid behaviours coexist. Second, the deformation states are not recoverable upon increasing/decreasing stresses and a rheological hysteresis is observed. Third, during the unloading branch of the stress ramp, an elastic recoil effect is systematically observed. The observation of a rheological hysteresis and of the elastic recoil effect may phenomenologically explain the observation of the fore-aft symmetry breaking of the flow patterns measured around a solid object settling in a Carbopol gel as well as the emergence of a negative wake effect similar to that observed more than two decades ago with viscoelastic fluids.

Motivated by the claim made by Dinkgreve and coworkers in Ref. [16] that the rheological hysteresis solely emerges when the Carbopol gel samples are over-stirred during preparation and the gel micro-structure is mechanically damaged, we focused in Sec. 3.2 on the microscopic visualisation of the Carbopol sample used in this study. As a first attempt in doing so, we have closely followed the fluorescent staining procedure of the Carbopol gel detailed in Sec. II of Ref. [16]. Whereas we could visualise some micro-structural features in an acid state (no measurable yield stress), Fig. 8(a), all the micro-structural details have simply vanished when the sample was brought to a neutral pH (measurable yield stress), Fig. 8(b). This prompted us to develop a more sophisticated fluorescent labelling protocol to bind covalently (not ionically by simply adding molecular dye to the Carbopol gel) molecules of Rhodamine 6G on the Carbopol molecules. By doing so, we were able to unequivocally demonstrate that the micro-structure of our gel was not broken during the preparation step (Fig. 10) meaning that the physical origins of the non “*model*” behavior of the Carbopol gel used in this study are different from the one advanced in Ref. [16].

The measurements of the shear rate during an increasing linear ramp of stresses ($\tau = Bt$) exhibit a clear dependence on the characteristic forcing time t_0 (the time per stress value) within the **(S)** and **(S+F)** deformation regimes, Fig. 12. On both the loading and the unloading branch, a plateau of the shear rate consistent with the Hooke’s law is observed within **(S)** regime.

The magnitude A of the rheological hysteresis observed in Fig. 7 decreases with increasing the characteristic forcing time t_0 as a power law $A \propto t_0^{-1}$, Fig. 14. This indicates that in the asymptotic limit of a steady state forcing $t_0 \rightarrow \infty$ the yielding behaviour of the Carbopol gel approaches the “*model*” yielding scenario illustrated in Fig. 1.

The phenomenological modelling of the yielding transition of the Carbopol gel is discussed in Sec. 3.5. First, we show that contrarily to the claim made in Ref. [16], the simple structural model proposed in Ref. [9] can not describe any of the key features of the solid-fluid transition, Sec. 3.5.1. Next, it is demonstrated in Sec. 3.5.2 that the phenomenological model proposed in Ref. [33] is able to describe both qualitatively and quantitatively the response of the gel during controlled stress ramps, Fig. 16, and steps in the rate of strain, Fig. 17.

The overall conclusion of this study is that the response of Carbopol gels subjected to stress does exhibit a number of features not accounted for within the “*model*” picture particularly around the solid-fluid transition: rheological hysteresis, elastic recoil during a controlled stress unloading process and stress overshoot. We emphasise once more that none of these features is related to a mechanical damage of the micro-structure of the gel. As the solid-fluid transition depends strongly on the rate the energy is injected into the system, one may safely state that Carbopol gels are not the “*model*” yield stress materials as considered during the past several decades but simply time dependent elasto-viscoplastic materials which, in the asymptotic limit of a steady state forcing, tend to behave as “*model*” yield stress materials.

5. Author contributions

The project was jointly designed by T.B. and V.B. The experiments were carried on by E.Y. The data were analysed jointly by E.Y. and T.B. The chemical protocol for the covalent labelling of the Carbopol micro-structure was designed jointly by M.H. and Z.S. The paper was written by T.B. All authors have participated in reading and improving the initial draft.

6. Acknowledgements

We acknowledge the Agence Nationale de la Recherche (ANR) for the financial support via project NaiMYS (ANR-16-CE06-0003). V.B. gratefully

acknowledges a visiting fellowship from Polytech Nantes. T.B. gratefully acknowledges a visiting fellowship from the Institute of Macromolecular Chemistry, Czech Academy of Sciences, Prague. One of us (T.B.) is deeply indebted to Professor John Tsamopoulos for a number of insightful discussions as well as for providing Fig. 2(b).

- [1] Arigo, M. T., McKinley, G. H., 1998. An experimental investigation of negative wakes behind spheres settling in a shear-thinning viscoelastic fluid. *Rheologica Acta* 37 (4), 307 – 327.
URL <http://dx.doi.org/10.1007/s003970050118>
- [2] Balmforth, N. J., Rust, A. C., 2009. Weakly nonlinear viscoplastic convection. *Journal of Non-Newtonian Fluid Mechanics* 158 (1-3), 36 – 45.
- [3] Baravian, C., Quemada, D., 1998. Correction of instrumental inertia effects in controlled stress rheometry. *The European Physical Journal - Applied Physics* 2 (2), 189–195.
- [4] Barnes, H. A., Feb. 1999. The yield stress—a review or ‘*παντα ρει*’—everything flows? *Journal of Non-Newtonian Fluid Mechanics* 81 (1-2), 133–178.
URL <http://www.sciencedirect.com/science/article/B6TGV-3VFOXWV-7/2/83e19640e8b341acf88ddd76ebe06ad7>
- [5] Barnes, H. A., Walters, K., 1985. The yield stress myth ? *Rheol. Acta* 24, 323–326.
- [6] Beris, A. N., Tsamopoulos, J. A., Armstrong, R. C., Brown, R. A., 1985. Creeping motion of a sphere through a Bingham plastic. *J.FluidMech.* 158, 219–244.
- [7] Blackwell, B. C., Ewoldt, R. H., 2014. A simple thixotropic-viscoelastic constitutive model produces unique signatures in large-amplitude oscillatory shear (laos). *Journal of Non-Newtonian Fluid Mechanics* 208-209, 27 – 41.
URL <http://www.sciencedirect.com/science/article/pii/S0377025714000469>
- [8] Burghelea, T., Moyers-Gonzalez, M., Sainudiin, R., 2017. A nonlinear dynamical system approach for the yielding behaviour of a viscoplastic material. *Soft Matter* 13, 2024–2039.
URL <http://dx.doi.org/10.1039/C6SM02361D>

- [9] Coussot, P., Nguyen, Q. D., Huynh, H. T., Bonn, D., Apr 2002. Avalanche behavior in yield stress fluids. *Phys. Rev. Lett.* 88, 175501.
URL <http://link.aps.org/doi/10.1103/PhysRevLett.88.175501>
- [10] Coussot, P., Nguyen, Q. D., Huynh, H. T., Bonn, D., 2002. Viscosity bifurcation in thixotropic, yielding fluids. *Journal of Rheology* 46 (3), 573–589.
URL <http://scitation.aip.org/content/sor/journal/jor2/46/3/10.1122/1.1459447>
- [11] Curran, S., Hayes, R., Afacan, A., Williams, M., Tanguy, P., 2002. Properties of carbopol solutions as models for yield-stress fluids. *Journal of Food Science* 67 (1), 176–180.
URL <http://dx.doi.org/10.1111/j.1365-2621.2002.tb11379.x>
- [12] de Souza Mendes, P. R., 2009. Modeling the thixotropic behavior of structured fluids. *Journal of Non-Newtonian Fluid Mechanics* 164 (1-3), 66 – 75.
URL <http://www.sciencedirect.com/science/article/pii/S0377025709001578>
- [13] de Souza Mendes, P. R., 2011. Thixotropic elasto-viscoplastic model for structured fluids. *Soft Matter* 7, 2471–2483.
URL <http://dx.doi.org/10.1039/C0SM01021A>
- [14] Dimitriou, C. J., Ewoldt, R. H., McKinley, G. H., 2013. Describing and prescribing the constitutive response of yield stress fluids using large amplitude oscillatory shear stress (laostress). *Journal of Rheology* (1978-present) 57 (1), 27–70.
URL <http://scitation.aip.org/content/sor/journal/jor2/57/1/10.1122/1.4754023>
- [15] Dimitriou, C. J., McKinley, G. H., 2014. A comprehensive constitutive law for waxy crude oil: a thixotropic yield stress fluid. *Soft Matter* 10, 6619–6644.
URL <http://dx.doi.org/10.1039/C4SM00578C>
- [16] Dinkgreve, M., Fazilati, M., Denn, M. M., Bonn, D., 2018. Carbopol: From a simple to a thixotropic yield stress fluid. *Journal of Rheology* 62 (3), 773–780.
URL <https://doi.org/10.1122/1.5016034>
- [17] Divoux, T., Barentin, C., Manneville, S., 2011. From stress-induced fluidization processes to herschel-bulkley behaviour in simple yield stress

- fluids. *Soft Matter* 7, 8409–8418.
 URL <http://dx.doi.org/10.1039/C1SM05607G>
- [18] Divoux, T., Barentin, C., Manneville, S., 2011. Stress overshoot in a simple yield stress fluid: An extensive study combining rheology and velocimetry. *Soft Matter* 7, 9335–9349.
 URL <http://dx.doi.org/10.1039/C1SM05740E>
- [19] Divoux, T., Grenard, V., Manneville, S., Jan 2013. Rheological hysteresis in soft glassy materials. *Phys. Rev. Lett.* 110, 018304.
 URL <http://link.aps.org/doi/10.1103/PhysRevLett.110.018304>
- [20] Divoux, T., Tamarii, D., Barentin, C., Manneville, S., May 2010. Transient shear banding in a simple yield stress fluid. *Phys. Rev. Lett.* 104, 208301.
 URL <http://link.aps.org/doi/10.1103/PhysRevLett.104.208301>
- [21] Dullaert, K., Mewis, J., 2006. A structural kinetics model for thixotropy. *J. Non-Newtonian Fluid Mech.* (139), 21–30.
- [22] Fragedakis, D., Dimakopoulos, Y., Tsamopoulos, J., 2016. Yielding the yield-stress analysis: a study focused on the effects of elasticity on the settling of a single spherical particle in simple yield-stress fluids. *Soft Matter* 12, 5378–5401.
 URL <http://dx.doi.org/10.1039/C6SM00480F>
- [23] Gonzalez, M. M., Burghlea, T., Mak, J., 2011. Linear stability analysis for plane-poiseuille flow of an elastoviscoplastic fluid with internal microstructure for large reynolds numbers. *Journal of Non-Newtonian Fluid Mechanics* 166 (9-10), 515 – 531.
- [24] Gutowski, I., Lee, D., de Bruyn, J., Frisken, B., 2012. Scaling and mesostructure of carbopol dispersions. *Rheologica Acta*, 1–1010.1007/s00397-011-0614-6.
 URL <http://dx.doi.org/10.1007/s00397-011-0614-6>
- [25] Harlen, O. G., 2002. The negative wake behind a sphere sedimenting through a viscoelastic fluid. *Journal of Non-Newtonian Fluid Mechanics* 108 (1), 411 – 430, numerical Methods Workshop S.I.
 URL <http://www.sciencedirect.com/science/article/pii/S0377025702001398>
- [26] Kebiche, Z., Castelain, C., Burghlea, T., 2014. Experimental investigation of the rayleigh–bénard convection in a yield stress fluid. *Journal*

of Non-Newtonian Fluid Mechanics 203, 9 – 23.

URL <http://www.sciencedirect.com/science/article/pii/S0377025713001882>

- [27] Møller, P. C. F., Fall, A., Bonn, D., 2006. Yield stress and thixotropy: on the difficulty of measuring yield stress in practice. *Soft Mater* 2, 274–283.
- [28] Oppong, F. K., de Bruyn, J. R., 2007. Diffusion of microscopic tracer particles in a yield-stress fluid. *J. Non-Newtonian Fluid Mech.* 142, 104–111.
- [29] Oppong, F. K., Rubatat, L., Frisken, B. J., Bailey, A. E., de Bruyn, J. R., 2006. Microrheology and structure of a yield-stress polymer gel. *Phys. Rev. E* 73, 041405.
- [30] Ovarlez, G., Cohen-Addad, S., Krishan, K., Goyon, J., Coussot, P., 2013. On the existence of a simple yield stress fluid behavior. *Journal of Non-Newtonian Fluid Mechanics* 193, 68 – 79.
- [31] Piau, J., 2007. Carbopol gels: Elastoviscoplastic and slippery glasses made of individual swollen sponges: Meso- and macroscopic properties, constitutive equations and scaling laws. *Journal of Non-Newtonian Fluid Mechanics* 144 (1), 1 – 29.
URL <http://www.sciencedirect.com/science/article/pii/S0377025707000687>
- [32] Poumaere, A., Moyers-Gonzalez, M., Castelain, C., Burghelea, T., 2014. Unsteady laminar flows of a carbopol gel in the presence of wall slip. *Journal of Non-Newtonian Fluid Mechanics* 205 (0), 28 – 40.
URL <http://www.sciencedirect.com/science/article/pii/S0377025714000147>
- [33] Putz, A. M. V., Burghelea, T. I., 2009. The solid-fluid transition in a yield stress shear thinning physical gel. *Rheol Acta* 48, 673–689.
- [34] Putz, A. M. V., Burghelea, T. I., Frigaard, I. A., Martinez, D. M., 2008. Settling of an isolated spherical particle in a yield stress shear thinning fluid. *Phys. Fluids* (20), 033102.
- [35] Quemada, D., 1998. Rheological modeling of complex fluids: III: Dilatant behaviour of stabilized suspensions. *Eur. Phys. J. AP* (3), 309–320.

- [36] Quemada, D., 1998. Rheological modeling of complex fluids: I: The concept of effective volume fraction revisited. *Eur. Phys. J. AP* (1), 119–127.
- [37] Quemada, D., 1999. Rheological modeling of complex fluids: IV: Thixotropic and "thixoelastic" behaviour. Start-up and stress relaxation, creep tests and hysteresis cycles. *Eur. Phys. J. AP* (5), 191–207.
- [38] Roussel, N., Le Roy, R., Coussot, P., 2004. Thixotropy modelling at local and macroscopic scales. *J. non-Newtonian Fluid Mech.* 117 (2-3), 85–95.
- [39] Sainudiin, R., Moyers-Gonzalez, M., Burghelea, T., 2014. A microscopic gibbs field model for the macroscopic behavior of a viscoplastic fluid. UCDMS Research Report 2014/1, 1–17.
URL http://www.math.canterbury.ac.nz/~r.sainudiin/preprints/20140825_MicroNNF.pdf
- [40] Sainudiin, R., Moyers-Gonzalez, M., Burghelea, T., 2015. A microscopic gibbs field model for the macroscopic yielding behaviour of a viscoplastic fluid. *Soft Matter* 11 (27), 5531–5545.
- [41] Saramito, P., 2007. A new constitutive equation for elastoviscoplastic fluid flows. *Journal of Non-Newtonian Fluid Mechanics* 145 (1), 1 – 14.
URL <http://www.sciencedirect.com/science/article/pii/S0377025707000869>
- [42] Souliès, A., Pruvost, J., Legrand, J., Castelain, C., Burghelea, T. I., 2013. Rheological properties of suspensions of the green microalga *Chlorella vulgaris* at various volume fractions. *Rheologica Acta* 52 (6), 589 – 605.
- [43] Tarlet, D., Younes, E., Roux, S., Levy, A., Burghelea, T., 2019. Stopping of a solid object in an elasto viscoplastic material. *Journal of Non-Newtonian Fluid Mechanics* 263, 120 – 129.
URL <http://www.sciencedirect.com/science/article/pii/S0377025718301150>
- [44] Weber, E., Moyers-Gonzalez, M., Burghelea, T. I., 2012. Thermorheological properties of a carbopol gel under shear. *Journal of Non-Newtonian Fluid Mechanics* 183-184 (0), 14 – 24.
URL <http://www.sciencedirect.com/science/article/pii/S0377025712001322>
- [45] Zhang, J., Vola, D., Frigaard, I. A., 2006. Yield stress effects on Rayleigh-Bénard convection. *J. Fluid Mech* 566, 389.